LETTERS
https://doi.org/10.1038/s42255-020-0173-1

nature metabolism

Check for updates

Type 1 diabetes progression is associated with loss of CD3$^+$CD56$^+$ regulatory T cells that control CD8$^+$ T-cell effector functions

Giuseppe Terrazzano[1,2,11], Sara Bruzzaniti[3,4,11], Valentina Rubino[1,2,11], Marianna Santopaolo[3], Anna Teresa Palatucci[1], Angela Giovazzino[2], Claudia La Rocca[3], Paola de Candia[5], Annibale Puca[5], Francesco Perna[6], Claudio Procaccini[3,7], Veronica De Rosa[3,7], Chiara Porcellini[2], Salvatore De Simone[3], Valentina Fattorusso[2], Antonio Porcellini[4], Enza Mozzillo[2], Riccardo Troncone[2,8], Adriana Franzese[2], Johnny Ludvigsson[9], Giuseppe Matarese[3,10] ✉, Giuseppina Ruggiero[2] ✉ and Mario Galgani[3,10] ✉

An unresolved issue in autoimmunity is the lack of surrogate biomarkers of immunological self-tolerance for disease monitoring. Here, we show that peripheral frequency of a regulatory T cell population, characterized by the coexpression of CD3 and CD56 molecules ($T_{R3\text{-}56}$), is reduced in individuals with new-onset type 1 diabetes (T1D). In three independent T1D cohorts, we find that low frequency of circulating $T_{R3\text{-}56}$ cells is associated with reduced beta-cell function and with the presence of diabetic ketoacidosis. Since autoreactive CD8$^+$ T cells mediate disruption of insulin-producing beta cells[1-3], we demonstrate that $T_{R3\text{-}56}$ cells can suppress CD8$^+$ T cell functions in vitro by reducing the levels of intracellular reactive oxygen species. The suppressive function, phenotype and transcriptional signature of $T_{R3\text{-}56}$ cells are also altered in children with T1D. Together, our findings indicate that $T_{R3\text{-}56}$ cells constitute a regulatory cell population that controls CD8$^+$ effector functions, whose peripheral frequency may represent a traceable biomarker for monitoring immunological self-tolerance in T1D.

T1D is an autoimmune disease characterized by T cell-mediated destruction of insulin-producing beta cells in the pancreas[2]. An unresolved issue in T1D is the lack of biomarkers able to track immunological self-tolerance and disease progression in autoimmune disorders such as T1D. The peripheral blood of healthy individuals contains a T-cell subset coexpressing CD3 and CD56 molecules[4], whose peripheral frequency has been associated with different pathological conditions[5,6]. We recently observed that the number of CD3$^+$CD56$^+$ T cells present at T1D diagnosis directly reflected residual beta-cell function one year later[7].

To gain further insight into the physiopathological relevance and the potential regulatory function of CD3$^+$CD56$^+$ T cells (herein defined as $T_{R3\text{-}56}$ cells), we first enumerated circulating $T_{R3\text{-}56}$ cells (see Supplementary Fig. 1 for the gating strategy used) in a large cohort (enrolled in the Campania region of Italy, herein the 'Italian cohort') of prepubescent children with T1D at disease onset ($n=128$), compared to healthy children ($n=113$; Supplementary Table 1). We found that children with T1D had reduced percentage and absolute number of $T_{R3\text{-}56}$ cells compared to those in healthy controls (Fig. 1a). The observed differences were maintained after adjusting the comparison for sex, age and body mass index (BMI) (Extended Data Fig. 1a). The lower frequency of circulating $T_{R3\text{-}56}$ cells in individuals with T1D was associated, at least in part, with their increased rate of necrotic death ($1.5\pm0.14\%$, $3.9\pm0.44\%$ for healthy individuals and individuals with T1D, respectively), while no difference was observed in apoptosis (Extended Data Fig. 1b).

Next, we asked whether $T_{R3\text{-}56}$ cells are associated with residual pancreatic beta-cell function (measured as circulating fasting C-peptide) in T1D at disease onset. To this end, we performed a bivariate analysis that revealed a positive correlation between peripheral frequency and absolute number of $T_{R3\text{-}56}$ cells and fasting C-peptide levels ($r=0.71$, $P<0.0001$; $r=0.57$, $P<0.0001$, respectively; Fig. 1b,c).

Since diabetic ketoacidosis (DKA), glycated haemoglobin (HbA1c) and daily insulin dose strongly influence T1D complication over time[8,9], we applied logistic regression modelling on these parameters and revealed that low percentages of $T_{R3\text{-}56}$ cells could predict DKA at disease onset (Extended Data Fig. 1c, left). Prognostic validity of the fitted model was evaluated by receiver operating characteristic (ROC) curve analysis and measured using the area under the curve (AUC) (Extended Data Fig. 1c, right). Low absolute counts of $T_{R3\text{-}56}$ cells were also associated with the presence of DKA (Extended Data Fig. 1d). Finally, the frequency and absolute numbers of $T_{R3\text{-}56}$ cells were not associated with either HbA1c values or daily insulin dose (Supplementary Fig. 2).

We corroborated our findings in postpubescent young adults with T1D at diagnosis (Italian cohort, $n=19$; Supplementary Table 2).

[1]Dipartimento di Scienze, Università degli Studi di Potenza, Potenza, Italy. [2]Dipartimento di Scienze Mediche Traslazionali, Università degli Studi di Napoli Federico II, Naples, Italy. [3]Laboratorio di Immunologia, Istituto per l'Endocrinologia e l'Oncologia Sperimentale G. Salvatore, Consiglio Nazionale delle Ricerche, Naples, Italy. [4]Dipartimento di Biologia, Università degli Studi di Napoli Federico II, Naples, Italy. [5]Istituto di Ricovero e Cura a Carattere Scientifico MultiMedica, Milan, Italy. [6]Dipartimento di Medicina Clinica e Chirurgia, Università degli Studi di Napoli Federico II, Naples, Italy. [7]Unità di Neuroimmunologia, Fondazione Santa Lucia, Rome, Italy. [8]European Laboratory for the Investigation of Food-Induced Disease, Università degli Studi di Napoli Federico II, Naples, Italy. [9]Division of Pediatrics, Department of Biomedical and Clinical Sciences, Linköping University and Crown Princess Victoria Children's Hospital, Linköping, Sweden. [10]Dipartimento di Medicina Molecolare e Biotecnologie Mediche, Università degli Studi di Napoli Federico II, Naples, Italy. [11]These authors contributed equally to this work: Giuseppe Terrazzano, Sara Bruzzaniti, Valentina Rubino. ✉e-mail: giuseppe.matarese@unina.it; giruggie@unina.it; mario.galgani@unina.it

Specifically, we observed that $T_{R3\text{-}56}$ cell frequency and absolute number were reduced compared to those in age-matched healthy individuals ($n=14$; Fig. 1d), were positively correlated with plasma levels of fasting C-peptide ($r=0.46$, $P=0.047$; $r=0.50$, $P=0.0369$, respectively; Fig. 1e,f) and were negatively associated with the presence of DKA (Extended Data Fig. 1e,f).

To further validate $T_{R3\text{-}56}$ cells as traceable biomarkers of T1D progression, we analysed an independent cohort of children with recent-onset T1D ($n=36$) recruited at Linköping University Hospital, Sweden (Supplementary Table 3). In this validation cohort (herein defined as the 'Swedish cohort'), bivariate analysis further confirmed that the frequency of circulating $T_{R3\text{-}56}$ cells was positively correlated with fasting C-peptide ($r=0.63$, $P<0.0001$; Fig. 2a).

Next, we measured the specificity of our findings in a third independent cohort of individuals with T1D ($n=44$) recruited at the European Laboratory for the Investigation of Food-Induced Disease, Università degli Studi di Napoli Federico II (Supplementary Table 4), where T1D at diagnosis was or was not associated with another autoimmune disorder/immune dysregulation (either autoimmune thyroiditis (AIT) or coeliac disease). Strikingly, at T1D diagnosis, in 23 out of 44 children (going to develop coeliac disease or AIT in the following 3 years), bivariate analysis confirmed a positive correlation between $T_{R3\text{-}56}$ cells and fasting C-peptide levels ($r=0.57$, $P=0.0043$) (Fig. 2b). Logistic regression modelling established that the peripheral percentages of $T_{R3\text{-}56}$ cells indicated the presence of DKA (Extended Data Fig. 2a). On the other hand, in 21 out of 44 children who, at T1D diagnosis, were already affected by either coeliac disease or AIT, $T_{R3\text{-}56}$ cells did not show a statistical correlation with fasting C-peptide levels ($r=-0.003$, $P=0.9901$; Fig. 2c), and were weakly associated with the presence of DKA (Extended Data Fig. 2b).

To exclude the notion that the association between $T_{R3\text{-}56}$ cells and C-peptide relied on metabolic alterations (that is, hyperglycaemia and DKA), which are both typical of T1D onset, we assessed their frequency in individuals with T1D ($n=31$) one year after T1D diagnosis when metabolic alterations had stabilized. In these individuals, we found that $T_{R3\text{-}56}$ cell frequency was positively correlated with plasma levels of fasting C-peptide ($r=0.53$, $P=0.0023$) and reflected residual beta-cell mass (Fig. 2d).

Finally, to rule out the possibility of a bias introduced by the presence of possible outliers in the peripheral frequency of $T_{R3\text{-}56}$ cells, analyses excluding these individuals were performed and revealed a statistical correlation between $T_{R3\text{-}56}$ cells and fasting C-peptide (Extended Data Fig. 3).

To investigate whether the frequency of $T_{R3\text{-}56}$ cells was associated with the presymptomatic stages of T1D, we measured the frequency of $T_{R3\text{-}56}$ cells in 51 at-risk individuals, siblings of individuals with T1D from our main Italian cohort, followed over time every 6 months from 2015. This included 35 autoantibody-negative (Ab^-), 9 autoantibody-positive (Ab^+) and 7 Ab^+ who reverted to Ab^- (Ab reverted) individuals. Interestingly, we observed that the frequency of $T_{R3\text{-}56}$ cells was significantly higher in Ab reverted individuals compared to healthy Ab^- and Ab^+ children (Fig. 2e). We also noticed a significant reduction of $T_{R3\text{-}56}$ cells in Ab^+ individuals compared to healthy individuals (Fig. 2e). In all, peripheral frequency of $T_{R3\text{-}56}$ cells can act as a specific, noninvasive T1D biomarker able to reflect disease progression and severity in T1D at onset and far from diagnosis. However, further investigations on larger cohorts of at-risk individuals are needed to confirm $T_{R3\text{-}56}$ cells as biomarkers of the early asymptomatic phase of disease.

Moreover, if T1D development was preceded by another immune-mediated disorder (either coeliac disease or AIT), $T_{R3\text{-}56}$ cells failed to predict T1D progression, probably because of confounding factors related to an already compromised immunological self-tolerance associated with the first autoimmune disorder.

Since a high frequency of $T_{R3\text{-}56}$ cells is associated with a preserved residual beta-cell reservoir, we hypothesized a possibly unexplored immune regulatory role for this cellular subset. To test this hypothesis, we first characterized $T_{R3\text{-}56}$ cells in adult healthy donors and subsequently assessed their function, surface phenotype and molecular profile in children with T1D. Specifically, we measured the capacity of flow-sorted human $T_{R3\text{-}56}$ cells to affect the proliferation of in vitro T-cell receptor (TCR)-stimulated human $CD8^+$ and $CD4^+$ T cells from adult healthy donors. Strikingly, we observed that $T_{R3\text{-}56}$ cells inhibited proliferation of both $CD8^+$ and $CD4^+$ T cells (Fig. 3a), with the main suppressive effect on the proliferation of the $CD8^+$ cell subset (Fig. 3a). These findings prompted us to focus on the ability of $T_{R3\text{-}56}$ cells to suppress the effector/cytotoxic functions of $CD8^+$ T lymphocytes. We evaluated the ability of $T_{R3\text{-}56}$ cells to control cytotoxicity of human $CD8^+$ T cells (effectors) against an allogeneic target (see experimental procedure in Supplementary Fig. 3). Specifically, compared with control cells, $T_{R3\text{-}56}$ cells suppressed the lytic capacity of $CD8^+$ effector cells at different effector:target ratios (Fig. 3b). Next, we further explored the regulatory activity of $T_{R3\text{-}56}$ cells on cytolytic T lymphocytes (CTLs), generated from $CD8^+$ T cells stimulated with recombinant human interleukin-2 (IL-2) in vitro[10,11] (see experimental procedure in Supplementary Fig. 4). CTLs were cocultured with $T_{R3\text{-}56}$ or control cells and stimulated for 4 h via TCR to evaluate cytotoxic activity (measured by lysosome-associated membrane glycoprotein 1 (LAMP-1/CD107a) expression as a readout of cytotoxicity[12,13]) and interferon-gamma (IFN-γ) production by CTLs (see experimental procedure in Supplementary Fig. 4 and gating strategy in Supplementary Fig. 5). $T_{R3\text{-}56}$ cells significantly suppressed CTL effector functions, while the addition of either natural killer (NK) or $CD8^+$ T cells (as the internal control), did not affect LAMP-1/

Fig. 1 | $T_{R3\text{-}56}$ cell enumeration predicts residual beta-cell function in individuals with T1D at disease onset. a, Percentage (left) and absolute number (right) of circulating $T_{R3\text{-}56}$ cells in prepubescent individuals with T1D ($n=128$ for percentage and n = 126 for absolute number, respectively) at disease onset (Italian cohort), compared to age- and sex-related healthy individuals ($n=113$). Data are presented as box plots (minimum, maximum, median, and 25th and 75th percentiles); each dot represents an individual. *$P<0.0001$ by two-tailed Mann–Whitney *U*-test. **b**, Scatter plot showing the positive correlation between the frequency of circulating $T_{R3\text{-}56}$ cells and serum levels of fasting C-peptide in prepubescent individuals (Italian cohort) affected by T1D ($n=128$) at disease onset; $r=0.71$, $P<0.0001$ by two-tailed Pearson's correlation. The red line indicates the regression and the shading indicates the confidence interval. **c**, Scatter plot showing the positive correlation between the absolute number of circulating $T_{R3\text{-}56}$ cells and serum levels of fasting C-peptide in prepubescent individuals with T1D ($n=126$) at disease onset from the Italian cohort; $r=0.57$, $P<0.0001$ by two-tailed Pearson's correlation. The red line indicates the regression and the shading indicates the confidence interval. **d**, Box plots indicating the percentage (left) and absolute number (right) of circulating $T_{R3\text{-}56}$ cells in postpubescent young adults with T1D ($n=19$ for percentage and $n=18$ for absolute number, respectively) at disease onset (Italian cohort), compared to age- and sex-matched healthy individuals ($n=14$). Each dot represents an individual. Data are shown as described for **a**. $^{a}P=0.0001$, *$P<0.0001$ by two-tailed Mann–Whitney U-test. **e**, Scatter plot showing the positive correlation between the frequency of circulating $T_{R3\text{-}56}$ cells and serum levels of fasting C-peptide in postpubescent young adults with T1D ($n=19$) at disease onset from the Italian cohort; $r=0.46$, $P=0.0477$ by two-tailed Pearson's correlation. The red line indicates the regression and the shading indicates the confidence interval. **f**, Scatter plot showing the correlation between the absolute number of circulating $T_{R3\text{-}56}$ cells and serum levels of fasting C-peptide in postpubescent young adults with T1D ($n=18$) from the Italian cohort; $r=0.50$, $P=0.0369$ by two-tailed Pearson's correlation. The red line indicates the regression and the shading indicates the confidence interval.

CD107a expression and IFN-γ production by CTLs (Fig. 3c). We also found that the suppressive functions of $T_{R3\text{-}56}$ cells were maintained in coculture with allogeneic CTLs (Extended Data Fig. 4a).

To identify the molecular mechanisms of $T_{R3\text{-}56}$ cell suppression, we assessed whether this function relied on cell-to-cell contact, secretion of soluble factors or both. Transwell experiments revealed

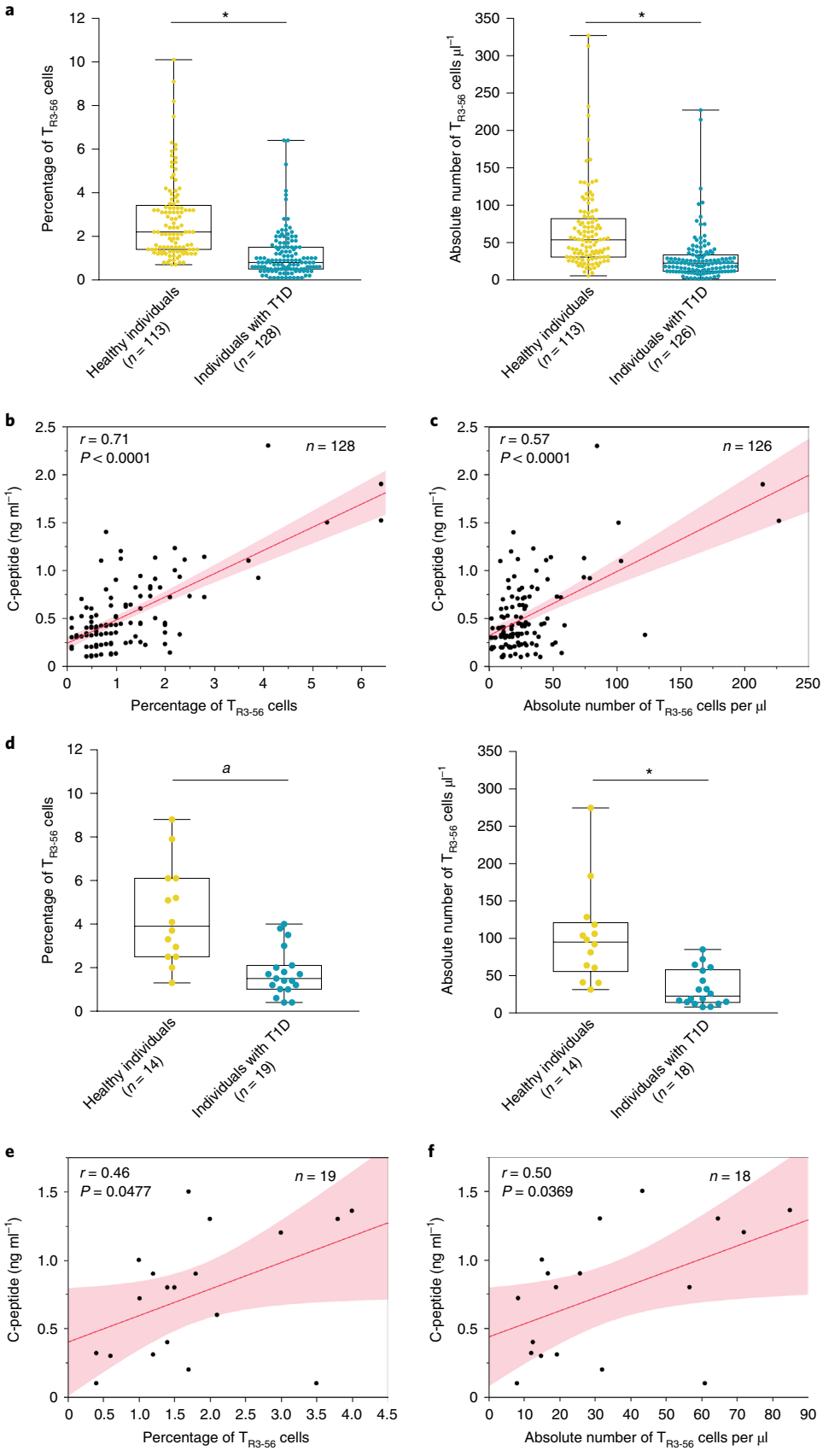

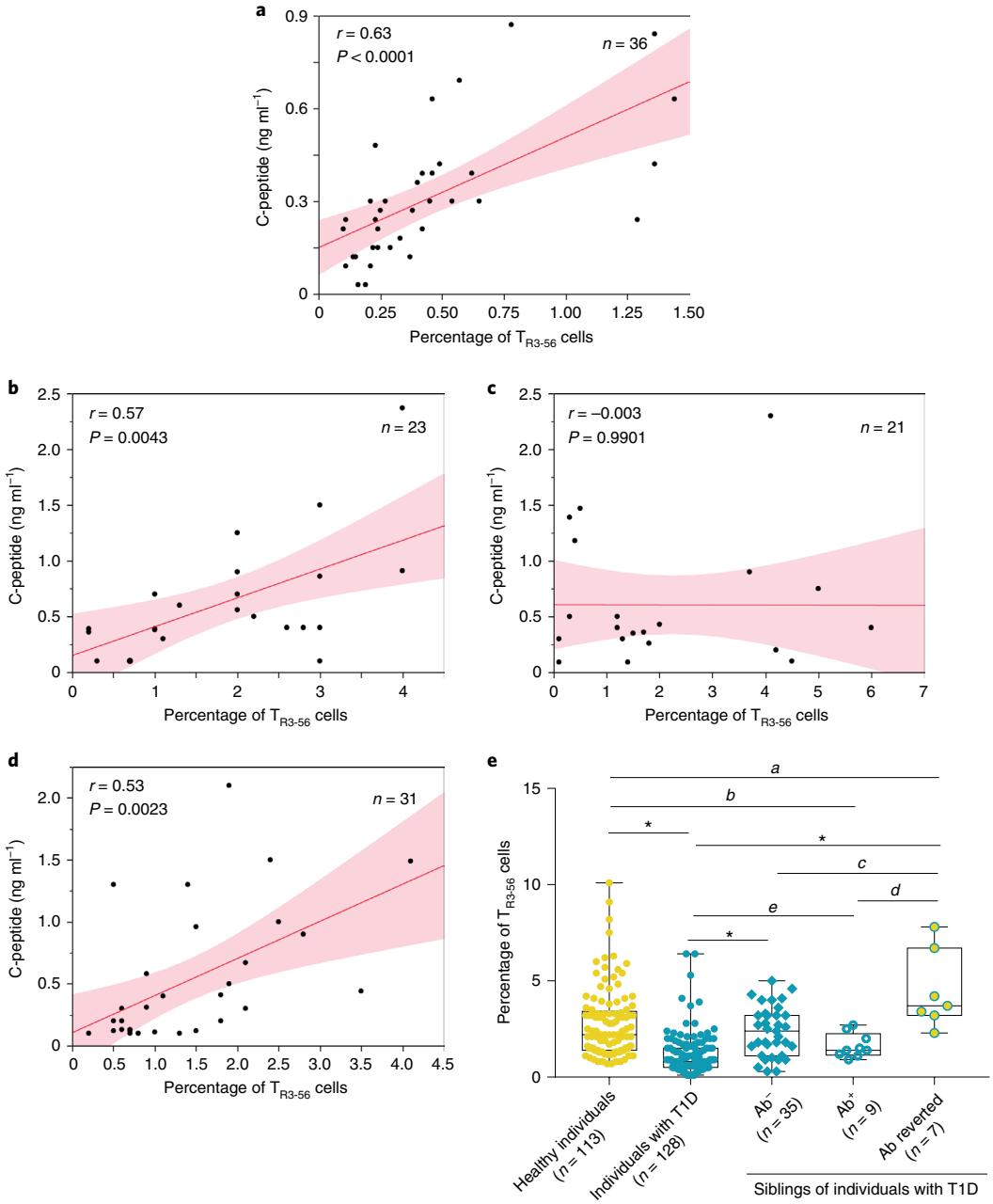

Fig. 2 | Validation and specificity of the predictive role of $T_{R3\text{-}56}$ cells. a, Scatter plot showing the positive correlation between the frequency of circulating $T_{R3\text{-}56}$ cells and serum levels of fasting C-peptide in a validation cohort (Swedish cohort) of children with T1D ($n=36$) at disease onset; $r=0.63$, $P<0.0001$ by two-tailed Pearson's correlation. The red line indicates the regression and the shading indicates the confidence interval. **b**, Scatter plot showing the positive correlation between the frequency of circulating $T_{R3\text{-}56}$ cells and serum levels of fasting C-peptide in a cohort of children with T1D who developed other autoimmune conditions after T1D diagnosis ($n=23$); $r=0.57$, $P=0.0043$ by two-tailed Pearson's correlation. The red line indicates the regression and the shading indicates the confidence interval. **c**, Scatter plot showing the absence of statistical correlation between the frequency of circulating $T_{R3\text{-}56}$ cells and serum levels of fasting C-peptide in children ($n=21$) who, at T1D diagnosis, were already affected by other autoimmune conditions (coeliac disease or AIT); $r=-0.003$, $P=0.9901$ by two-tailed Pearson's correlation. The red line indicates the regression and the shading indicates the confidence interval. **d**, Scatter plot showing positive correlation between the frequency of circulating $T_{R3\text{-}56}$ cells and serum levels of fasting C-peptide in T1D subjects one year after diagnosis (Italian cohort) (n=31); $r=0.53$, $P=0.0023$ by two-tailed Pearson's correlation. Red line indicates regression line and shading indicates confidence interval. **e**, Box plot indicating the frequency of $T_{R3\text{-}56}$ cells in healthy individuals ($n=113$), children with T1D at diagnosis ($n=128$) and 51 at-risk siblings of individuals with T1D: 35 Ab^-, 9 Ab^+ and 7 Ab^+ reverted to Ab^- (Ab reverted) individuals. Data are presented as box plots (minimum, maximum, median, and 25th and 75th percentiles); each dot represents an individual. $^aP=0.0084$; $^bP=0.0456$; $^cP=0.006$; $^dP=0.0007$; $^eP=0.0106$; $^*P<0.0001$ by two-tailed Mann–Whitney *U*-test.

that $T_{R3\text{-}56}$ cells did not exert regulatory activity when separated from CTLs (Fig. 3d and Extended Data Fig. 4b). Therefore, their contact-mediated suppressive activity was independent of the expression of CD56 molecules (Extended Data Fig. 4c).

Reactive oxygen species (ROS)-mediated signalling has been frequently associated with degranulation processes and IFN-γ production by CTLs[14,15]. We studied dynamic changes of cytosolic and mitochondrial ROS levels on TCR stimulation of CTLs

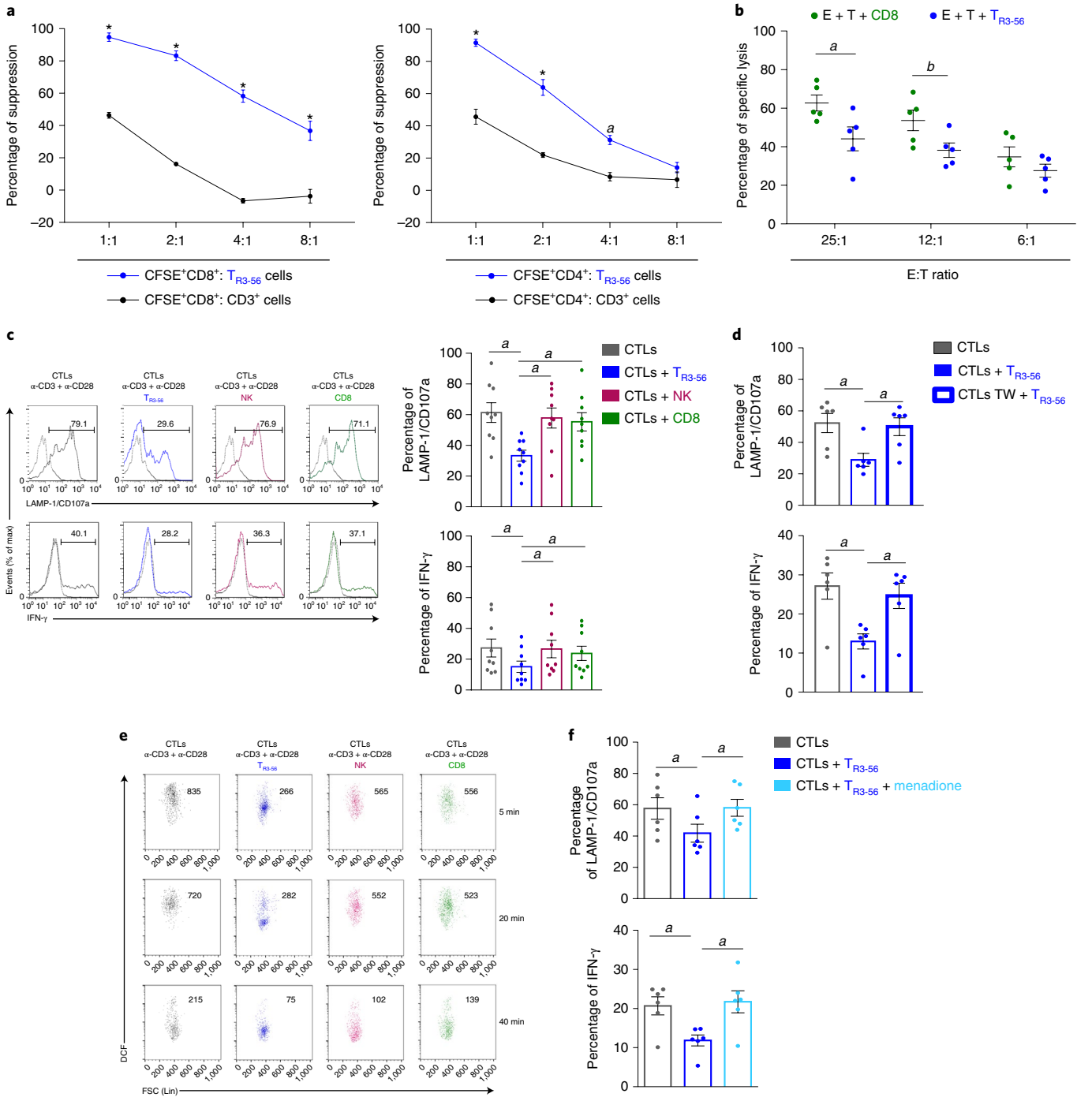

Fig. 3 | T_{R3-56} cells regulate $CD8^+$ effector functions by modulating intracellular ROS levels. a, Suppression exerted by T_{R3-56} (blue) or control cells on the proliferation of CFSE-labelled $CD8^+$ (left) and CFSE-labelled $CD4^+$ (right) lymphocytes stimulated with TCR for 72 h in vitro, at different ratios. Data are from independent experiments: $n = 6$ for T_{R3-56} cells and $n = 3$ for $CD3^+$ cells. The error bars represent the s.e.m. $^aP = 0.0013$; $^*P < 0.0001$ by two-way ANOVA Bonferroni-corrected for multiple comparisons. **b**, Cytolytic activity of CTLs against allogeneic PBMCs. PBMCs (target) were CFDA-labelled and cocultured for 3 h with allogenic CTLs, in the presence of either T_{R3-56} or control cells (see also Supplementary Fig. 3). Data are from five independent experiments ($n = 5$). $^aP = 0.0376$; $^bP = 0.0460$ by two-tailed Student's *t*-test. Data are expressed as the mean ± s.e.m. **c**, Left: LAMP-1/CD107a and IFN-γ staining of CTLs after 4 h stimulation with TCR alone (grey), in the presence of T_{R3-56} (blue) or control cells (see also Supplementary Fig. 4). Data are from one representative experiment out of nine. The dotted lines indicate unstimulated cells. The numbers indicate the percentage of positive cells. Right: cumulative data from nine independent experiments. Data are expressed as the mean ± s.e.m. $^aP = 0.0039$ by two-tailed Wilcoxon matched pairs test. **d**, LAMP-1/CD107a and IFN-γ from CTLs stimulated for 4 h with TCR alone (grey), in the presence of T_{R3-56} cells (blue) or when T_{R3-56} cells were separated in the Transwell plate (bold blue). Data are expressed as the mean ± s.e.m. Data are from six independent experiments ($n = 6$). $^aP = 0.013$ by two-tailed Wilcoxon matched pairs test. **e**, Kinetics of DCF staining, as a measure of intracellular ROS levels, of CTLs TCR-stimulated alone (grey) with T_{R3-56} cells (blue), or in the presence of control cells. The numbers in the plot show the mean fluorescence intensity. Data are from one representative experiment out of three. FSC, forward scattering. **f**, LAMP-1/CD107a and IFN-γ production by CTLs stimulated for 4 h with TCR alone (grey) or in the presence of T_{R3-56} cells (blue); the light blue boxes indicate coculture of T_{R3-56} cells with menadione-pretreated CTLs. Data are from six independent experiments. Data are expressed as the mean ± s.e.m. $^aP = 0.013$ by two-tailed Wilcoxon matched pairs test.

cultured with $T_{R3\text{-}56}$ cells. Cytosolic CTL ROS levels, evaluated by 2′,7′-dichlorodihydrofluorescein diacetate (DCF) staining, were significantly reduced by $T_{R3\text{-}56}$ cells (Fig. 3e); control cells (NK or CD8$^+$ T cells) did not influence cellular ROS levels in CTLs (Fig. 3e). Conversely, $T_{R3\text{-}56}$ cells did not affect mitochondrial-derived ROS in CTLs, as testified by MitoSOX staining (Supplementary Fig. 6). To confirm the role of cellular ROS in mediating $T_{R3\text{-}56}$ cell regulatory activity, we took advantage of the ability of menadione, an analogue of 1,4-naphthoquinone, to generate intracellular ROS via redox cycling[16,17]. $T_{R3\text{-}56}$ cells did not suppress LAMP-1/CD107a expression and IFN-γ of menadione-pretreated CTLs (Fig. 3f and Extended Data Fig. 5). In addition, menadione per se did not induce in vitro CTL activation in the absence of TCR stimulation (Extended Data Fig. 5). To note, treatment with the ROS inhibitor *N*-acetyl-l-cysteine (NAC), completely blocked CTL activation[18], suggesting that $T_{R3\text{-}56}$ cells control CD8$^+$ responses by modulating cytosolic ROS.

Finally, adult $T_{R3\text{-}56}$ cells were also characterized for metabolic features (glycolysis and oxidative phosphorylation) and their transcriptional signature. Seahorse analysis revealed that on TCR stimulation, $T_{R3\text{-}56}$ cells have a distinct metabolic phenotype compared to those of NK, CD8$^+$ and CD4$^+$ cells, by preferentially utilizing oxidative phosphorylation as the main cellular bioenergetic source (Supplementary Fig. 7). Microarray analysis of RNA from $T_{R3\text{-}56}$ cells revealed their distinct transcriptomic signature, compared to those of NK, CD3$^+$CD56$^-$ and CD8$^+$ subsets (Supplementary Fig. 8).

Compelling experimental evidence supports the central role of T lymphocytes in immune-mediated damage of beta cells in T1D[19–21]. Autoreactive CD8$^+$ T lymphocytes kill beta-cells through the release of cytolytic granules and by producing tissue-damaging pro-inflammatory cytokines[22,23]. Since specific regulatory networks targeting CD8$^+$ T cell functions are still poorly understood in T1D, we explored whether human $T_{R3\text{-}56}$ cells are involved in T1D pathogenesis. We evaluated suppressive capability, phenotype, cytokine production and transcriptomic molecular signature of $T_{R3\text{-}56}$ cells isolated from individuals with recent-onset T1D compared to those isolated from healthy children. Notably, $T_{R3\text{-}56}$ cells isolated from individuals newly diagnosed with T1D had decreased ability to modulate TCR-dependent LAMP-1/CD107a expression of autologous CTLs (Fig. 4a). This impaired suppressive function was not due to the presence of suppression-resistant CD8$^+$ T cells in individuals with T1D, since CTLs from T1D was sensitive to the regulatory activity of $T_{R3\text{-}56}$ cells from healthy individuals (Fig. 4b). These results indicate that the suppressive capability of $T_{R3\text{-}56}$ cells is impaired in children with T1D at diagnosis.

Surface phenotypic analysis revealed that $T_{R3\text{-}56}$ cells from children with recent-onset T1D were comparable to those from healthy controls for CD4, CD8, CD45RA, CD45RO and CD27 expression, whereas CD28 surface levels were significantly higher in $T_{R3\text{-}56}$ cells from individuals with T1D (Fig. 4c and Extended Data Fig. 6a). Also, $T_{R3\text{-}56}$ cells from children with T1D had reduced surface expression of activating/inhibitory receptors (CD94, NKG2A, NKG2C, NKG2D, DNAM-1 and CD16) (ref. [24]) and cytotoxicity-related molecules (granzyme B)[23], compared to those from healthy children (Fig. 4c). On the other hand, $T_{R3\text{-}56}$ cells from children with recent-onset T1D expressed increased surface levels of chemokine receptor homing cells in the pancreas, such as CXCR3, CXCR4 and CCR7 (Fig. 4c) (refs. [25–27]). Low or moderate levels of the main regulatory T cell (T_{reg}) cell-associated markers[28], such as CD25, the transcription factor FOXP3, CTLA-4, CD39, GITR and PD-1 were expressed on $T_{R3\text{-}56}$ cells from both controls and individuals with T1D (Supplementary Fig. 9).

Finally, fluorescence-activated cell sorting (FACS) analysis revealed that $T_{R3\text{-}56}$ cells from both healthy controls and individuals with T1D are distinct from the invariant *i*NKT subset[29,30], do not express the Vα24/Vβ11 TCR chains and display a heterogeneous β-TCR repertoire, since they are not CD1d-restricted (Extended Data Fig. 6a,b).

After 48 h of TCR stimulation, multiplex cytokine analysis showed that $T_{R3\text{-}56}$ cells from individuals with new-onset T1D had reduced amounts of IFN-γ, IL-2, IL-4, IL-13, IL-21, IL-22 and tumour necrosis factor-alpha (TNF-α) compared with those from healthy controls (Fig. 4d). On the other hand, $T_{R3\text{-}56}$ cells from children with T1D secreted increased amounts of IL-15 and IL-17A (Fig. 4d), while no significant differences were observed for other cytokines, such as IL-8, IL-9, IL-10, IL-31 and TNF-β (Fig. 4d). Furthermore, an unbiased high-throughput analysis (RNA sequencing (RNA-seq)) of the transcriptome expressed by $T_{R3\text{-}56}$ cells from children with T1D compared to age- and sex-matched healthy controls revealed the dysregulation of several genes that may contribute to T1D-dependent functional impairment of this cell subset. In particular, we concentrated our attention on genes ($n=33$; see Fig. 4e) whose mean level was decreased by more than twofold in T1D cells compared to cells from healthy counterparts: the majority of these genes ($n=23$) encoded proteins functionally linked to the membrane, suggesting a rearrangement of the cell surface in

Fig. 4 | Functional and molecular dysregulation of $T_{R3\text{-}56}$ cells from children with recent-onset T1D. a, LAMP-1/CD107a staining of CTLs TCR-stimulated for 4 h alone (grey) or with autologous $T_{R3\text{-}56}$ cells (blue) from one representative healthy individual (top) and an individual with T1D (bottom). Right: suppression of LAMP-1/CD107a in CTLs from individuals with T1D ($n=11$) and healthy individuals ($n=15$) in presence of autologous $T_{R3\text{-}56}$ cells. Each dot represents an individual. Data are expressed as the mean ± s.e.m. $^aP=0.0456$ by two-tailed Mann–Whitney *U*-test. **b**, LAMP-1/CD107a expression in CTLs, from an individual with T1D, TCR-stimulated for 4 h alone (left), or in the presence of autologous (middle) or allogeneic (right) $T_{R3\text{-}56}$ cells from a healthy control. Data are from one representative experiment out of three. The dotted lines indicate unstimulated CTLs. The numbers indicate the percentage of positive cells. **c**, Expression of molecules on $T_{R3\text{-}56}$ cells from healthy individuals and individuals with T1D. Data are from $n=16$ healthy individuals, $n=24$ individuals with T1D for all molecules except for CD94 ($n=16$ healthy individuals, $n=22$ individuals with T1D), NKG2C ($n=16$ healthy individuals, $n=21$ individuals with T1D) and CXCR4 ($n=14$ healthy individuals, $n=19$ individuals with T1D). Each dot represents an individual. Data are expressed as the mean ± s.e.m. $^aP=0.04$; $^bP=0.0442$; $^cP=0.0294$; $^dP=0.044$; $^eP=0.0062$; $^fP=0.0147$; $^gP=0.0211$; $^hP=0.0041$; $^iP=0.0010$; $^*P<0.0001$ by two-tailed Mann–Whitney *U*-test. **d**, Cytokines released by $T_{R3\text{-}56}$ cells TRC-stimulated for 48 h in vitro from healthy and individuals with T1D ($n=4$ healthy individuals, $n=6$ individuals with T1D for IFN-γ, IL-8 and IL-9; $n=5$ healthy individuals, $n=6$ individuals with T1D for IL-4, IL-13 and IL-31; $n=4$ healthy individuals and individuals with T1D for IL-15 and IL-17A; $n=6$ healthy individuals, $n=9$ individuals with T1D for IL-2; $n=6$ healthy individuals, $n=10$ individuals with T1D for IL-10; $n=6$ healthy individuals, $n=8$ individuals with T1D for IL-23; $n=5$ healthy individuals, $n=7$ individuals with T1D for IL-22; $n=5$ healthy individuals and individuals with T1D for TNF-α; $n=6$ healthy individuals, $n=7$ individuals with T1D for TNF-β). Each dot represents an individual. Data are expressed as the mean ± s.e.m. $^aP=0.0381$; $^bP=0.0132$; $^cP=0.0476$; $^dP=0.0043$; $^eP=0.0286$; $^fP=0.0426$; $^gP=0.0366$; $^hP=0.0317$ by two-tailed Mann–Whitney *U*-test. **e**, Heatmap of *z*-scored RNA-seq expression values of 33 genes with a $\log_2$ fold change < –1.0 when $T_{R3\text{-}56}$ cells from healthy individuals and individuals with T1D are compared ($n=3$ for group). **f**, Protein–protein interaction network reconstructed from the STRING database and differentially expressed transcripts ($\log_2$ fold change < –1.0 as in **e**) identified by comparing RNA-seq profiles from the $T_{R3\text{-}56}$ cells of both groups ($n=3$ for group) by non-parametric/permutation-based and multiple testing correction according to Benjamini–Hochberg method. The 23 genes leading to a significant enrichment of the cellular component 'membrane' (GO:0016020, false discovery rate = 0.0059) are shown in blue.

T1D (Fig. 4f). Specifically, $T_{R3\text{-}56}$ cells from individuals newly diagnosed with T1D expressed lower levels of the *GPR65* gene, which has been genetically associated with autoimmune disorders[31], and the *KLRB1/CD161* and *KLRC1/NKG2-A* genes, two killer cell lectin-like receptors, described to function as inhibitory determinants in human NK cells[32,33]. Furthermore, in T1D $T_{R3\text{-}56}$ cells, we also observed decreased expression of genes encoding proteins related to regulatory functions, such as *LAPTM4B* (ref. [34]) and *HPGD*[35].

In summary, this study reveals that $T_{R3\text{-}56}$ cells may represent a disease biomarker with a previously undisclosed role in human T1D. In three independent cohorts—from Italy and Sweden–of individuals with new-onset T1D, we found that a lower frequency of this cellular subset is associated with reduced insulin-secreting capacity and undesirable disease outcome, such as DKA. Also, we found that $T_{R3\text{-}56}$ cells possess a certain degree of specificity for T1D since their enumeration failed to predict disease progression when T1D was preceded by another autoimmune disease as the confounding factor. Moreover, $T_{R3\text{-}56}$ cells were associated to C-peptide levels later on from the initial T1D diagnosis (one year later), when metabolic alterations would have been normalized. Taken together, our results revealed functional, phenotypic and molecular impairments in $T_{R3\text{-}56}$ cells isolated at T1D onset suggesting a 'general' dysregulation of this cellular subset in T1D. This was confirmed by reduced expression of inhibitory/activating receptors and genes encoding proteins

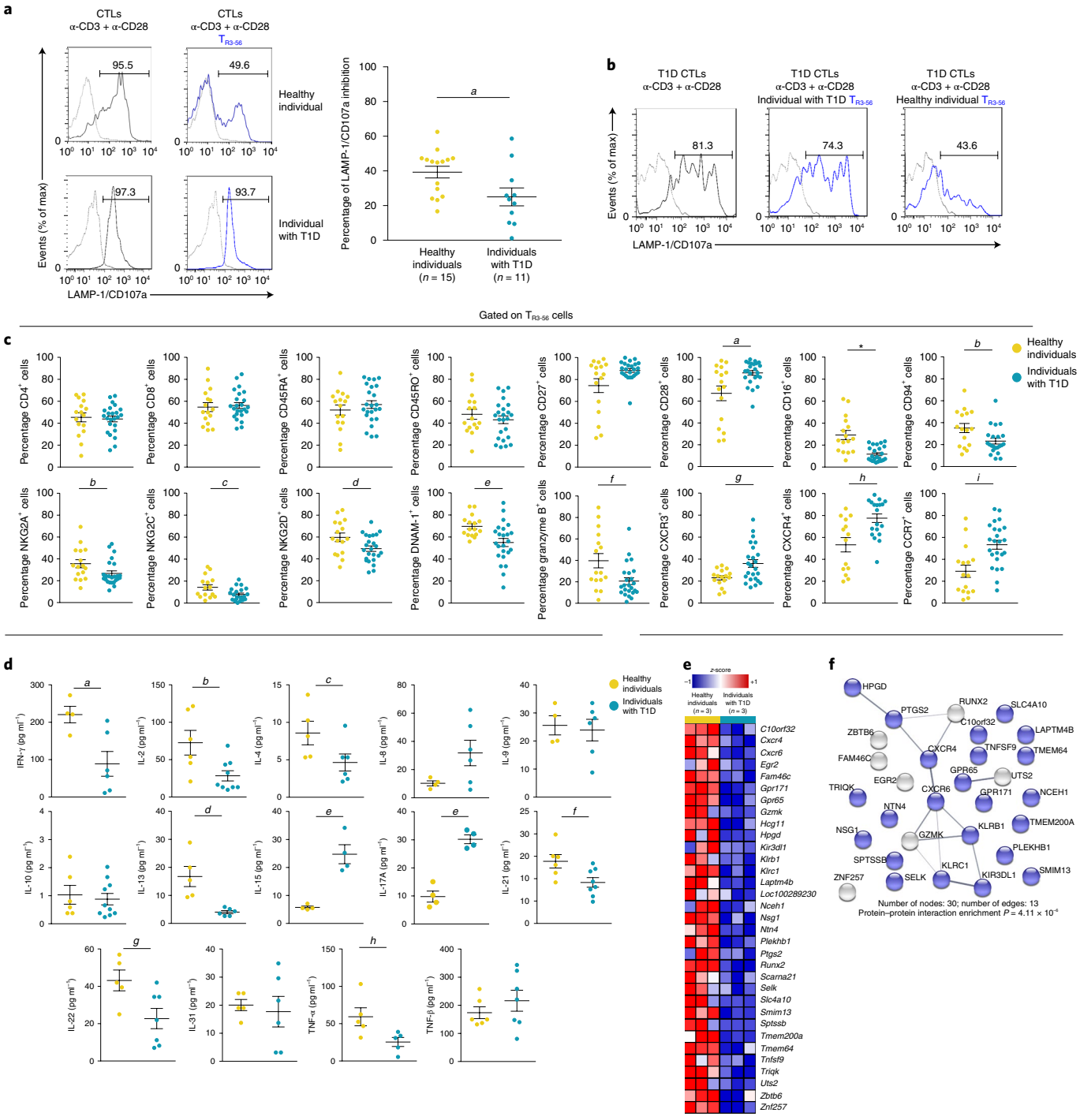

involved in canonical T_{reg} cell-mediated suppressive functions (that is, *LPTMB*4 and *HPGD*)[32–35]. In an integrated view, defects of $T_{R3\text{-}56}$ cells were associated with attack of pancreatic beta cells by islet-specific autoreactive $CD8^+$ T-cell clones, affecting residual insulin production and influencing T1D progression (Extended Data Fig. 7). Furthermore, $T_{R3\text{-}56}$ cell counts may represent a valuable criterion to monitor disease progression, while also improving the stratification of individuals for T1D trials and the identification of at-risk individuals with prediabetes during the asymptomatic phase of the disease. More research is needed to further strengthen our findings; studies are in progress also in other autoimmune disorders to expand the role of $T_{R3\text{-}56}$ cells in immunological self-tolerance and their potential translational relevance in a wider perspective. In conclusion, we propose a model wherein, under healthy conditions, $T_{R3\text{-}56}$ cells might participate in immune regulation to preserve tissue integrity of insulin-producing beta cells (Extended Data Fig. 7). An alteration in number and/or function of this cellular subset could lead to beta-cell damage and loss of endogenous insulin production (measured as fasting C-peptide), thus allowing the seed of autoimmunity to take root (Extended Data Fig. 7).

Methods

Healthy individuals and individuals with T1D. The diagnosis of T1D was defined according to the Global International Diabetes Federation/International Society for Pediatric and Adolescent Diabetes Guidelines for Diabetes in Childhood and Adolescence[36] and included symptoms of diabetes in addition to casual plasma glucose concentration ≥11.1 mmol l^{-1} (200 mg dl^{-1}), or fasting plasma glucose ≥7.0 mmol l^{-1} (≥126 mg dl^{-1}), or 2 h postload glucose ≥11.1 mmol l^{-1} (≥200 mg dl^{-1}) during an oral glucose tolerance test, and HbA1c ≥6.5 (ref. [36]). Individuals with recent-onset T1D and individuals one year after T1D diagnosis from the Italian cohort were recruited at the Dipartimento di Scienze Mediche Traslazionali, Sezione di Pediatria, Università di Napoli Federico II (A. Franzese). Individuals with T1D from the validation Swedish cohort were recruited at the Crown Princess Victoria Children's Hospital, University Hospital, Linköping, Sweden (J. Ludvigsson). Peripheral blood mononuclear cells (PBMCs) were isolated and frozen at the Division of Pediatrics, Department of Biomedical and Clinical Sciences, Linköping University, Sweden. Individuals from the cohort who developed other autoimmune diseases (coeliac disease or AIT) before or after T1D diagnosis were recruited at European Laboratory for the Investigation of Food-Induced Disease, Università di Napoli Federico II (R. Troncone). Coeliac disease was diagnosed in accordance with the 1990 European Society for Pediatric Gastroenterology Hepatology, and Nutrition guidelines[37]; diagnosis of AIT was based on the presence of high levels of antithyroid antibodies (anti-thyroperoxidase and/or anti-thyroglobulin), normal or low thyroid function (thyroxine, thyroid-stimulating hormone), together with a heterogenicity and hypoechogenicity of thyroid parenchyma at ultrasound examination[38]. At-risk individuals, siblings of children with T1D, were recruited at the Dipartimento di Scienze Mediche Traslazionali, Sezione di Pediatria, Università di Napoli Federico II. Ab^+ individuals were positive for at least two autoantibodies. Healthy children were recruited at the Dipartimento di Scienze Mediche Traslazionali, Sezione di Pediatria, Università di Napoli Federico II (A. Franzese). Blood samples from individuals with recent-onset T1D were collected 10 d after glycaemic stabilization by treatment with exogenous insulin (glucose values between 3.5 and 10 mmol l^{-1} or 80 and 180 mg dl^{-1}) and all were positive for at least two anti-islet autoantibodies. Healthy individuals were matched for sex, age and BMI with individuals with T1D and selected according to the following criteria: fasting blood glucose of <5.5 mmol l^{-1} (<100 mg dl^{-1}); negative personal and familial history of autoimmune disorders; and negativity for islet autoantibodies at the 99th percentile. Individuals with T1D and healthy individuals with recent vaccinations or infections were excluded from the study. (See Supplementary Tables 1–4 for the demographic and clinical characteristics of the healthy and T1D cohorts.)

The institutional review board of the Ethics Committee of the Università di Napoli Federico II approved the study (protocol nos. 200/16 and N.161/18). Approval by the Research Ethics Committee of Linköping University was also obtained (no. Dnr 02-482). All adult participants, or the parents of participating children, provided written informed consent. The study complies with all relevant ethical regulations.

Laboratory testing. Blood samples from individuals with T1D, at-risk siblings and healthy individuals were withdrawn at 8:00 into heparinized BD Vacutainers and processed within the following 4 h. Serum or plasma were obtained after centrifugation and kept at −80 °C until use. Fasting C-peptide levels were measured in duplicate serum samples, at the same time for all samples, using a commercial enzyme-linked immunosorbent assay (ELISA) kit (Merck Millipore). The results for each assay were validated and high- and low-level control samples were included. Glucose levels were measured using the enzymatic hexokinase method; HbA1c levels were measured by high-performance liquid chromatography (HLC-723 G7; Tosoh Bioscience). Islet autoantibodies (glutamic acid decarboxylase, islet antigen 2, insulin and zinc transporter 8 autoantibodies), transglutaminase immunoglobulin A and antithyroid antibodies (anti-thyroperoxidase and/or anti-thyroglobulin) were measured by commercial ELISA (Pantec). Whole blood cells were analysed with a clinical-grade haemocytometer to determine absolute lymphocyte numbers in each sample. The remaining part of blood samples was processed; after Ficoll-Paque (GE Healthcare Life Sciences) gradient centrifugation, PBMCs were obtained.

For the validation T1D Swedish cohort, blood samples were processed at the Division of Pediatrics, Department of Clinical and Experimental Medicine, Medical Faculty, Linköping University, Sweden. PBMCs were obtained and cryopreserved in liquid nitrogen. An aliquot was shipped to our laboratory at the Istituto per l'Endocrinologia e l'Oncologia Sperimentale (IEOS)-Consiglio Nazionale delle Ricerche (CNR) and kept in liquid nitrogen until use. Nitrogen-cryopreserved PBMCs from the Swedish cohort were thawed as follows: cryogenic vials containing frozen cells were removed from liquid nitrogen storage and placed into a 37 °C water bath; vials were gently swirled in the 37 °C water bath until there was a small amount of ice left in the vial. Prewarmed complete growth medium (Roswell Park Memorial Institute (RPMI) 10% FCS) was added dropwise to the cryogenic vial containing the thawed cells. After centrifugation, cells were resuspended in complete growth medium and used for flow cytometry staining. Viability was assessed after defrosting and was on average >85%.

Flow cytometry and cell isolation. PBMCs from healthy human donors, individuals with T1D and at-risk siblings of individuals with T1D were stained with the following antibodies to evaluate $T_{R3\text{-}56}$ cells: FITC mouse anti-human CD3 (clone UCHT1; BD Biosciences); PE-Cy7 mouse anti-human CD56 (clone B159; BD Biosciences).

To evaluate $T_{R3\text{-}56}$ cell death, PBMCs were stained with the following antibodies: FITC annexin V (BD Biosciences); PE-Cy7 mouse anti-human CD56; APC mouse anti-human CD3 (clone UCHT1; BD Biosciences). Propidium iodide (BD Biosciences) and annexin V buffer (BD Biosciences) were used to stain cells according the manufacturer's instructions.

Multiparametric flow cytometry was used to evaluate surface markers on $T_{R3\text{-}56}$ cells from PBMCs (all BD Biosciences, unless stated otherwise): FITC or APC mouse anti-human CD3; PE or APC mouse anti-human CD4 (clone RPA-T4); BV421 mouse anti-human CD8 (clone RPA-T8); PE mouse anti-human CD16 (clone 3G8); BV510 mouse anti-human CD27 (clone M-T271); PE mouse anti-human CD28 (clone CD28.2); APC mouse anti-human CD45 (clone HI30); FITC anti-human CD45RA (clone REA562; Miltenyi Biotec); APC mouse anti-human CD45RO (clone UCHL1); PeCy7 or APC mouse anti-human CD56 (clone NCAM16.2); APC mouse anti-human CD94 (clone HP-3D9); BB700 rat anti-human CCR7 (clone 3D12); BV510 mouse anti-human CD183 (clone 1C6/CXCR3); BB700 mouse anti-human CD184 (clone 12G5); BV510 mouse anti-human DNAM-1 (clone DX11); BB700 mouse anti-human NKG2A (clone 131411); BV510 mouse anti-human CD159c/NKG2C (clone 134591); APC mouse anti-human CD314/NKG2D (clone 1D11); PE-labelled CD1d tetramers loaded with α-galactosyl ceramide (Proimmune); PE-labelled CD1d negative control tetramers (Proimmune); FITC anti-human Vα24 (clone C15; Beckman Coulter); BV421 mouse anti-human granzyme B (clone GB11); PECy7 mouse anti-human CD25 (clone M-A251); BV421 mouse anti-human CD279/PD-1 (clone EH12.1); PE mouse anti-human FoxP3 (clone 259D/C7); APC mouse anti-human CD152/CTLA-4 (clone BN13); APC mouse anti-human CD39 (clone TU66); BV421 mouse anti-human GITR (clone V27-580). The FITC- and PE-labelled monoclonal antibodies against TCR Vβ epitopes were: anti-human Vβ1; Vβ2; Vβ3; Vβ4; Vβ5.1; Vβ5.2; Vβ5.3; Vβ7.1; Vβ7.2; Vβ8; Vβ9; Vβ11; Vβ12; Vβ13.1; Vβ13.2; Vβ13.6; Vβ14; Vβ16; Vβ17; Vβ18; Vβ20; Vβ21.3; Vβ22; and Vβ23 (all from Beckman Coulter). Granzyme B expression was performed by using the Fixation/Permeabilization Solution Kit BD Cytofix/Cytoperm (BD Biosciences), according to the manufacturer's instructions. Staining for intracellular factors was performed by using the FOXP3 fixation and permeabilization Buffer Kit (BD Biosciences), according to the manufacturer's instructions. Samples were acquired by using a FACSCanto II equipped with two lasers (BD Biosciences) with at least 3×10^4 events in the lymphocyte gate. To evaluate positive events, fluorescence minus one controls were used to set the gate; non-viable cells were detected by 7-amino-actinomycin D viability staining (BD Biosciences). See Supplementary Fig. 1 for the gating strategy of $T_{R3\text{-}56}$ cells. Cytofluorimetric analyses were performed using the FlowJo software v.10.

Human $CD3^+CD56^+$ ($T_{R3\text{-}56}$), $CD3^-CD56^+$ (NK), $CD3^+CD56^-$, $CD4^+$ and $CD8^+$ T cells were isolated from the PBMCs of healthy human donors and individuals with T1D using high-performance cell sorting (BD FACSJazz; BD Biosciences) at the IEOS-CNR Sorting Facility, after staining with the following antibodies (all from BD Biosciences): FITC mouse anti-human CD3; APC anti-human CD56; APC mouse anti-human CD4; and APC anti-human CD8 or by magnetic cell separation with $CD3^+CD56^+$ MicroBeads (Miltenyi Biotec), the Dynabeads CD8 Positive Isolation Kit (Thermo Fisher Scientific) and Dynabeads Regulatory

$CD4^+CD25^+$ T Cell Kit (Thermo Fisher Scientific). The purity of isolated cells was 95–99% as reported in the figures.

Proliferation assays. To analyse cell division, flow-sorted $CD4^+$ and $CD8^+$ T cells were labelled with 5,6-carboxyfluorescein diacetate succinimidyl ester (CFSE; Thermo Fischer Scientific) before culturing[39]. To assess cell proliferation, 3×10^4 $CD4^+$ or $CD8^+$ cells were cultured for 72 h in the presence of $T_{R3\text{-}56}$ cells (or $CD3^+CD56^-$ control cells) stimulated with anti-CD3 plus anti-CD28 MicroBeads (0.2 beads per cell; Thermo Fisher Scientific) at different cell ratios (1:1, 1:2, 1:4, 1:8), as described previously[39]. All tests were performed in the presence of RPMI 1640 medium (Thermo Fisher Scientific) supplemented with 5% heat-inactivated AB human serum (Euroclone). CFSE analyses were performed using the BD FACSCanto II and FlowJo software.

Cytotoxicity assays. To obtain CTLs directed against allogeneic targets, flow-sorted $CD8^+$ cells (purity > 95%) from adult healthy donors (effectors) were cultured with 30 Gy-irradiated allogeneic PBMCs (stimulators) for 10 d with regular recombinant human IL-2 supplementation (20 IU ml^{-1}); allogeneic targets were obtained by anti-CD3 treatment and recombinant human IL-2 expansion of stimulator PBMCs. The specific cytotoxicity of effector cells was measured using the 5,6-carboxyfluorescein diacetate (CFDA) cytotoxicity assay (Molecular Probes). Briefly, target cells were labelled with CFDA mixed with effector cells at different effector to target cell (E:T) ratios and incubated at 37 °C for 3 h in 96-well round bottom plates (Falcon; BD). The specific lysis of target cells was calculated as follows: percentage of specific lysis = (CT−TE/CT) × 100, where CT is the mean number of fluorescent target cells in control tubes and TE is the mean number of fluorescent cells in target plus effector tubes[40,41]. $T_{R3\text{-}56}$ cells (or $CD8^+$ control cells) and effector CTLs were cocultured (at a 1:1 ratio) to evaluate the ability of $T_{R3\text{-}56}$ cells to suppress the lytic capacity of effector CTLs against the CFDA-labelled allogeneic target (see experimental procedure in Supplementary Fig. 3).

Degranulation assay, LAMP-1/CD107a expression and IFN-γ production. To obtain activated CTLs, flow-sorted $CD8^+$ T cells were cultured for 36 h in RPMI 1640 (Thermo Fisher Scientific) supplemented with 5% AB human serum (Euroclone) in the presence of recombinant human IL-2 (Roche) at 200 IU ml^{-1}. After 36 h, CTLs were labelled with BV421-conjugated anti-human CD8 and then cultured alone or in the presence of freshly flow-sorted $T_{R3\text{-}56}$, NK and $CD8^+$ T lymphocytes at different ratios, with or without TCR stimulation (1 bead per cell) in 96-well round bottom plates. PE-conjugated anti-human LAMP-1/CD107a (clone H4A3; BD Biosciences) was added to the cell culture for the whole culture period (4 h).

To avoid extracellular cytokine export, cultures were performed in the presence of 5 μg ml^{-1} of brefeldin A (Sigma-Aldrich), as described in Terrazzano et al.[42]; for the LAMP-1/CD107a experiments, brefeldin A was added in the last 3 h of culturing. For IFN-γ production, CTLs were cultured as described earlier, while 5 μg ml^{-1} of brefeldin A was added to the cell culture for the whole culture period (4 h)[12,13,42]. Then, to evaluate IFN-γ expression, samples were fixed and permeabilized (Cytofix-Cytoperm) and stained for PE mouse anti-human IFN-γ (clone B27; BD Biosciences), according to the manufacturer's instructions.

For the Transwell experiments, the coculture of $T_{R3\text{-}56}$ cells and CTLs was performed under the conditions outlined earlier using Transwell inserts (Corning Life Sciences) in 24-well round bottom plates. For the degranulation assay in the presence of CD56, recombinant human NCAM-1/CD56 protein (R&D Systems) was used (10 ng ml^{-1}). The mouse IgG2a 345.134 monoclonal antibody (control), which recognizes a glycoprotein widely expressed on human leucocytes[43], was a kind gift of S. Ferrone and was used as described earlier.

In all experiments, non-viable cells were detected by 7-amino-actinomycin D viability staining; both LAMP-1/CD107a expression and IFN-γ production were evaluated in labelled CTLs, using the fluorescence values of unstimulated CTLs (medium) as negative values to identify positive gates, as described in the experimental procedure shown in Supplementary Fig. 4 and the gating strategy in Supplementary Fig. 5. All experiments were performed under autologous conditions except when indicated. Experiments in adult healthy individuals were performed by coculturing 1×10^5 CTLs and 1×10^5 $T_{R3\text{-}56}$ or control cells; the experiments involving children with T1D and their controls were performed by coculturing at least 3×10^4 CTLs and 3×10^4 $T_{R3\text{-}56}$ or control cells because of the reduced volume of blood obtained from children and because of the reduced frequency of this $T_{R3\text{-}56}$ population in T1D.

ROS production. For intracellular ROS production, CTLs were stained using DCF (Sigma-Aldrich). Briefly, CTLs were stained with DCF and cultured alone or with $T_{R3\text{-}56}$ or control cells in the presence of anti-CD3 and anti-CD28; ROS production was detected after 5, 20 and 40 min of culture. Induction of intracellular ROS was obtained by treating CTLs with menadione (0.05 μM). Mitochondrial ROS were measured by MitoSOX Red Mitochondrial Superoxide Indicator (Thermo Fisher Scientific), according to the manufacturer's instructions. DCF and MitoSoX levels were evaluated by flow cytometry using the BD FACSCanto II and FlowJo software.

Seahorse analyses. Metabolic profile was evaluated in $T_{R3\text{-}56}$, NK, $CD3^+CD56^-$ and $CD8^+$ cells from adult healthy individuals in the presence of anti-CD3 and anti-CD28 MicroBeads (1 bead per cell; Thermo Fisher Scientific) for 1 h. Real-time measurement of extracellular acidification and oxygen consumption rates was performed using a Seahorse XFe96 Analyzer (Agilent Technologies). Specifically, cells were plated in XFe96 plates at a concentration of 2×10^5 cells per well and cultured with RPMI 1640 medium supplemented with 5% AB human serum. The extracellular acidification rate was measured in XF DMEM Medium (Agilent Technologies) under basal conditions and in response to 10 mM of glucose, 5 μM of oligomycin and 100 mM of 2DG (all from Sigma-Aldrich). The oxygen consumption rate was measured in XF DMEM Medium (supplemented with 10 mM of glucose, 2 mM of L-glutamine and 1 mM of sodium pyruvate), under basal conditions and in response to 5 μM of oligomycin, 1.5 μM of carbonyl cyanide-*4*-(trifluoromethoxy)phenylhydrazone and 1 μM of antimycin A and rotenone (all from Sigma-Aldrich). The Seahorse experiments were done under the following assay conditions: 3 min mixture; 3 min wait; and 3 min measurement.

Transcriptome analysis. For microarray analysis, flow-sorted cell populations ($T_{R3\text{-}56}$, NK, $CD3^+CD56^-$, $CD8^+$) isolated from healthy adults ($n=3$ biological replicates for each cell population obtained from adult healthy individuals) were quantified through microarray-based human Affymetrix Clariom S Assays (Eurofins Genomics), which provide extensive coverage of all known well-annotated genes (21,448 gene probes for 19,525 unique annotated genes). The raw intensity values were background-corrected, $\log_2$-transformed and quantile-normalized using the robust multi-array average algorithm. Data were imported and analysed using Multiple Experiment Viewer. Sample similarity was described by multivariate principal component analysis and Pearson's correlation. For supervised sample clustering, significant genes were selected using one-way analysis of variance (ANOVA), followed by Pearson's correlation. To identify a $T_{R3\text{-}56}$ cell-specific gene expression pattern, we selected genes that had a consistent $\log_2$ fold change (either >+1 or <−1) compared to all other populations evaluated (NK, $CD3^+CD56^-$ and $CD8^+$ cells) and a significant Student's *t*-test ($P<0.05$) for all three comparisons: $T_{R3\text{-}56}$ versus NK, $T_{R3\text{-}56}$ versus $CD3^+CD56^-$ and $T_{R3\text{-}56}$ versus $CD8^+$ T cells.

For next-generation sequencing analysis, RNA-seq was performed by IGA Technology Services. Total RNA was extracted from $T_{R3\text{-}56}$ cells isolated from either healthy individuals ($n=3$) or individuals with recent-onset T1D ($n=3$) using the RNeasy Micro Kit (QIAGEN) according to the manufacturer's instructions. RNA samples were then quantified and quality-tested using an Agilent 2100 Bioanalyzer RNA assay (Agilent Technologies) or Caliper (PerkinElmer). Libraries were prepared using the Ovation SoLo RNA-seq Library Preparation Kit (NuGEN), according to the manufacturer's instructions, and checked with both a Qubit 2.0 Fluorometer (Thermo Fisher Scientific) and an Agilent Bioanalyzer DNA assay (Agilent Technologies) or Caliper. Sequencing was performed on single-end 75 base pair mode on a NextSeq 500 (Illumina); the number of reads ranged from 29.1×10^6 to 32.5×10^6. Raw data were processed by Bcl2Fastq v.2.0.2 of the Illumina pipeline for format conversion and demultiplexing; lower-quality bases and adaptors were removed using the ERNE (v.1.4.6)[44] and Cutadapt (v. 1.16)[45] software. Reads were then deduplicated based on a unique molecular identifier composed of eight random bases for unambiguous identification of unique library molecules by an IGA Technology Services proprietary script; they were aligned on the GRCh38 genome/transcriptome reference with STAR (v.3.2.6)[46]. Full-length transcripts representing multiple spliced variants for each gene locus were assembled and quantified by StringTie (v. 1.3.4d)[47]. RNA-seq data were preprocessed by counting the overlap of reads with genes using htseq-count (v.0.9.1)[48]; DESeq2 (v.1.14.1)[49] was used to perform comparisons between the expression levels of genes and transcripts. Normalization was performed using the median of ratios method[50] and statistical significance was determined using a Wald test[49].

Cytokine assessment. A total of 40,000 flow-sorted $T_{R3\text{-}56}$ cells from healthy individuals and individuals with T1D were cultured with RPMI 1640 medium supplemented with 5% autologous serum in the presence of anti-CD3 and anti-CD28 MicroBeads (0.1 bead per cell; Thermo Fisher Scientific). After 48 h, supernatant was collected and stored at −20 °C until use. Cytokine production was analysed using a bead-based multianalyte immunoassay (Thermo Fisher Scientific) according to the manufacturer's recommendations; it was then was measured using multiplex technology (Luminex 200; Luminex). The xPONENT v.3.1 software (Luminex) was used for data acquisition.

Statistical analysis. Modelling and statistical analysis of data were done using the Statistical Discovery software (JMP v.6.0.3) and Prism 7 (GraphPad Software). Comparisons were performed by Mann–Whitney *U*-test, Student's *t*-test, one-way ANOVA, two-way ANOVA Bonferroni-corrected for multiple comparisons and Wilcoxon matched pairs test as shown. Correlation analyses were performed using Pearson's correlation. A linear model was used to adjust the sex, age and BMI comparison variables. We applied the ROUT ($Q=0.1\%$) method to identify outliers.

For all analyses, we used two-tailed tests with $P<0.05$ denoting statistical significance. A univariate logistic regression model was fitted to predict DKA at T1D diagnosis as follows: individuals with T1D were dichotomized based on

the presence (Yes) or absence (No) of DKA at disease diagnosis. The prognostic validity of the fitted model was evaluated by ROC curve analysis and measured using the AUC. The black line represents the ROC curve derived from sensitivity (the probability that an X value is a true positive) versus 1-specificity (the probability that an X value is a false positive). The yellow line indicates the optimal combination of sensitivity and specificity according to the Youden criterion. The optimal combination between sensitivity and specificity is represented by the intercept between the ROC curve and the yellow line.

Reporting Summary. Further information on research design is available in the Nature Research Reporting Summary linked to this article.

Data availability

The data that support the findings of this study are available from the corresponding authors upon request. Transcriptional data of the $T_{R3\text{-}56}$, NK, $CD3^+CD56^-$ and $CD8^+$ cells from adult healthy individuals can be found in the Gene Expression Omnibus database under accession code GSE106082. Transcriptional data the of $T_{R3\text{-}56}$ cells from children with T1D and healthy children can also be found in the Gene Expression Omnibus database under accession code GSE134916. Source data for Figs. 1–4 and Extended Data Figs. 1, 2, 3 and 6 are included with this paper.

Received: 24 September 2019; Accepted: 17 January 2020;
Published online: 17 February 2020

References

1. Liblau, R. S., Wong, F. S., Mars, L. T. & Santamaria, P. Autoreactive CD8 T cells in organ-specific autoimmunity: emerging targets for therapeutic intervention. *Immunity* **17**, 1–6 (2002).
2. Coppieters, K. T. et al. Demonstration of islet-autoreactive CD8 T cells in insulitic lesions from recent onset and long-term type 1 diabetes patients. *J. Exp. Med.* **209**, 51–60 (2012).
3. Culina, S. et al. $CD8^+$ T cell frequencies in the pancreas, but not in blood, distinguish type 1 diabetic patients from healthy donors>. *Sci. Immunol.* **3**, eaao4013 (2018).
4. Schmidt, R. E., Murray, C., Daley, J. F., Schlossman, S. F. & Ritz, J. A subset of natural killer cells in peripheral blood displays a mature T cell phenotype. *J. Exp. Med.* **1**, 351–356 (1986).
5. Zhou, J. et al. High circulating $CD3^+CD56^+CD16^+$ natural killer-like T cell levels predict a better IVF treatment outcome. *J. Reprod. Immunol.* **97**, 197–203 (2013).
6. Diao, H. et al. A possible role for NKT-like cells in patients with chronic hepatitis B during telbivudine treatment. *Immunol. Lett.* **160**, 65–71 (2014).
7. Galgani, M. et al. Meta-immunological profiling of children with type 1 diabetes identifies new biomarkers to monitor disease progression. *Diabetes* **62**, 2481–2491 (2013).
8. Atkinson, M. A. et al. How does type 1 diabetes develop? The notion of homicide or β-cell suicide revisited. *Diabetes* **60**, 1370–1379 (2011).
9. Beato-Víbora, P. I. & Tormo-García, M. Á. Glycemic control and insulin requirements in type 1 diabetic patients depending on the clinical characteristics at diabetes onset. *Endocr. Res.* **39**, 86–90 (2014).
10. Pipkin, M. E. et al. Interleukin-2 and inflammation induce distinct transcriptional programs that promote the differentiation of effector cytolytic T cells. *Immunity* **32**, 79–90 (2010).
11. Kalia, V. et al. Prolonged interleukin-2Rα expression on virus-specific CD8+ T cells favors terminal-effector differentiation in vivo. *Immunity* **32**, 91–103 (2010).
12. Alter, G., Malenfant, J. M. & Altfeld, M. CD107a as a functional marker for the identification of natural killer cell activity. *J. Immunol. Methods* **294**, 15–22 (2004).
13. Wagner, J. A. et al. $CD56^{bright}$ NK cells exhibit potent antitumor responses following IL-15 priming. *J. Clin. Invest.* **127**, 4042–4058 (2017).
14. Yi, J. S., Holbrook, B. C., Michalek, R. D., Laniewski, N. G. & Grayson, J. M. Electron transport complex I is required for $CD8^+$ T cell function. *J. Immunol.* **177**, 852–862 (2006).
15. Bai, A. et al. NADH oxidase-dependent CD39 expression by $CD8^+$ T cells modulates interferon gamma responses via generation of adenosine. *Nat. Commun.* **9**, 8819 (2015).
16. Nazarewicz, R. R., Bikineyeva, A. & Dikalov, S. I. Rapid and specific measurements of superoxide using fluorescence spectroscopy. *J. Biomol. Screen.* **18**, 498–503 (2013).
17. Criddle, D. N. et al. Menadione-induced reactive oxygen species generation via redox cycling promotes apoptosis of murine pancreatic acinar cells. *J. Biol. Chem.* **281**, 40485–40492 (2006).
18. Terrazzano, G. et al. T cell activation induces CuZn superoxide dismutase (SOD)-1 intracellular re-localization, production and secretion. *Biochim. Biophys. Acta* **1843**, 265–274 (2014).
19. Wicker, L. S. et al. Type 1 diabetes genes and pathways shared by humans and NOD mice. *J. Autoimmun.* **25**, 29–33 (2005).
20. Roep, B. O. The role of T-cells in the pathogenesis of Type 1 diabetes: from cause to cure. *Diabetologia* **46**, 305–321 (2003).
21. Dirice, E. et al. Increased β-cell proliferation before immune cell invasion prevents progression of type 1 diabetes. *Nat. Metab.* **1**, 509–518 (2019).
22. Pugliese, A. Autoreactive T cells in type 1 diabetes. *J. Clin. Invest.* **127**, 2881–2891 (2017).
23. Pinkse, G. G. M. et al. Autoreactive CD8 T cells associated with β cell destruction in type 1 diabetes. *Proc. Natl Acad. Sci. USA* **102**, 18425–18430 (2005).
24. Sivori, S. et al. Human NK cells: surface receptors, inhibitory checkpoints, and translational applications. *Cell. Mol. Immunol.* **16**, 430–441 (2019).
25. Tan, T. G., Mathis, D. & Benoist, C. Singular role for T-BET^+CXCR3^+ regulatory T cells in protection from autoimmune diabetes. *Proc. Natl Acad. Sci. USA* **113**, 14103–14108 (2016).
26. van Halteren, A. G., Kardol, M. J., Mulder, A. & Roep, B. O. Homing of human autoreactive T cells into pancreatic tissue of NOD-scid mice. *Diabetologia* **48**, 75–82 (2005).
27. Shan, Z., Xu, B., Mikulowska-Mennis, A. & Michie, S. A. CCR7 directs the recruitment of T cells into inflamed pancreatic islets of nonobese diabetic (NOD) mice. *Immunol. Res.* **58**, 351–357 (2014).
28. Rudensky, A. Y. Regulatory T cells and Foxp3. *Immunol. Rev.* **241**, 260–268 (2011).
29. Godfrey, D. I. & Kronenberg, M. Going both ways: immune regulation via CD1d-dependent NKT cells. *J. Clin. Invest.* **114**, 1379–1388 (2004).
30. Kuylenstierna, C. et al. NKG2D performs two functions in invariant NKT cells: direct TCR-independent activation of NK-like cytolysis and co-stimulation of activation by CD1d. *Eur. J. Immunol.* **41**, 1913–1923 (2011).
31. Wirasinha, R. C. et al. GPR65 inhibits experimental autoimmune encephalomyelitis through $CD4^+$ T cell independent mechanisms that include effects on iNKT cells. *Immunol. Cell Biol.* **96**, 128–136 (2018).
32. Lin, Y.-L. & Lin, S.-C. Analysis of the CD161-expressing cell quantities and CD161 expression levels in peripheral blood natural killer and T cells of systemic lupus erythematosus patients. *Clin. Exp. Med.* **17**, 101–109 (2017).
33. Mingari, M. C., Pietra, G. & Moretta, L. Immune checkpoint inhibitors: anti-NKG2A antibodies on board. *Trends Immunol.* **40**, 83–85 (2019).
34. De Simone, M. et al. Transcriptional landscape of human tissue lymphocytes unveils uniqueness of tumor-infiltrating T regulatory cells. *Immunity* **45**, 1135–1147 (2016).
35. Schmidleithner, L. et al. Enzymatic activity of HPGD in T_{reg} cells suppresses T_{conv} cells to maintain adipose tissue homeostasis and prevent metabolic dysfunction. *Immunity* **50**, 1232–1248.e14 (2019).
36. Craig, M. E., Hattersley, A. & Donaghue, K. C. Definition, epidemiology and classification of diabetes in children and adolescents. *Pediatr. Diabetes* **10**, 3–12 (2009).
37. Revised criteria for diagnosis of coeliac disease. Report of Working Group of European Society of Paediatric Gastroenterology and Nutrition. *Arch. Dis. Child.* **65**, 909–911 (1990).
38. Hanley, P., Lord, K. & Bauer, A. J. Thyroid disorders in children and adolescents: a review. *JAMA Pediatr.* **170**, 1008–1019 (2016).
39. Bruzzaniti, S. et al. An immunometabolic pathomechanism for chronic obstructive pulmonary disease. *Proc. Natl Acad. Sci. USA* **116**, 15625–15634 (2019).
40. McGinnes, K., Chapman, G., Marks, R. & Penny, R. A fluorescence NK assay using flow cytometry. *J. Immunol. Methods* **86**, 7–15 (1986).
41. Tallerico, R. et al. Human NK cells selective targeting of colon cancer-initiating cells: a role for natural cytotoxicity receptors and MHC class I molecules. *J. Immunol.* **190**, 2381–2390 (2013).
42. Terrazzano, G. et al. Differential involvement of CD40, CD80, and major histocompatibility complex class I molecules in cytotoxicity induction and interferon-gamma production by human natural killer effectors. *J. Leukoc. Biol.* **72**, 305–311 (2002).
43. Sabbatini, M. et al. Oscillatory mTOR inhibition and T_{reg} increase in kidney transplantation. *Clin. Exp. Immunol.* **182**, 230–240 (2015).
44. Del Fabbro, C., Scalabrin, S., Morgante, M. & Giorgi, F. M. An extensive evaluation of read trimming effects on Illumina NGS data analysis. *PLoS ONE* **8**, e85024 (2013).
45. Martin, M. Cutadapt removes adapter sequences from high-throughput sequencing reads. *EMBnet J.* **17**, 10–12 (2011).
46. Dobin, A. et al. STAR: ultrafast universal RNA-seq aligner. *Bioinformatics* **29**, 15–21 (2013).
47. Pertea, M. et al. StringTie enables improved reconstruction of a transcriptome from RNA-seq reads. *Nat. Biotechnol.* **33**, 290–295 (2015).
48. Anders, S., Pyl, P. T. & Huber, W. HTSeq: a Python framework to work with high-throughput sequencing data. *Bioinformatics* **31**, 166–169 (2015).
49. Love, M. I., Huber, W. & Anders, S. Moderated estimation of fold change and dispersion for RNA-seq data with DESeq2. *Genome Biol.* **15**, 550 (2014).
50. Anders, S. & Huber, W. Differential expression analysis for sequence count data. *Genome Biol.* **11**, R106 (2010).

Acknowledgements

We thank M. Montagna and all members of the IEOS-CNR for their technical support, and M. Carrara and F. Marabita for assistance in the transcriptomic analysis. This paper was supported by grants from the Juvenile Diabetes Research Foundation (grant no. 2-SRA-2018-479-S-B to M.G.; grant no. 1-SRA-2018-477-S-B to P.D.C); the European Foundation for the Study of Diabetes (EFSD/JDRF/Lilly Programme 2016 to M.G.); the National Multiple Sclerosis Society (grant no PP-1804-30725 to M.G.); Fondazione Italiana Sclerosi Multipla (grant no. 2016/R/18 to G.M.; grant no. 2018/R/4 to V.D.R.); Ministero della Salute (grant no. GR-2016-02363725 to V.D.R.); Università degli Studi di Napoli Federico II (STAR Program Linea 1–2018 to V.D.R.); European Research Council menTORingTregs grant no. 310496 to G.M.); Telethon (grant no. GGP 17086 to G.M.); Grant Fondazione Italiana Sclerosi Multipla (grant no. 2018/S/5 to G.M.); and the Italian Ministry of Health Giovani Ricercatori (grant no. GR-2016-02363749 to C. Procaccini). This work has also been supported by Italian Ministry of Health Ricerca Corrente - IRCCS MultiMedica.

Author contributions

S.B., V.R., M.S., A.T.P., A.G., C.L.R. and S.D.S. performed the experiments and data analyses. F.P. and S.B. performed the flow cytometry experiments and data analyses. S.B., V.R., M.S., G.T., G.R., A. Porcellini, V.D.R., C. Procaccini and M.G. analysed the data and interpreted the results. A. Puca and P.D.C. analysed the transcriptional data. V.D.R., A. Porcellini and C. Procaccini were involved in the discussion about the data. J.L., C. Porcellini, V.F., E.M., R.T. and A.F. provided the patient samples and were involved in the discussion about the data. P.D.C., G.T., G.R., J.L., G.M. and M.G. designed the study and wrote the manuscript.

Competing interests

The authors declare no competing interests.

Additional information

Extended data is available for this paper at https://doi.org/10.1038/s42255-020-0173-1.

Supplementary information is available for this paper at https://doi.org/10.1038/s42255-020-0173-1.

Correspondence and requests for materials should be addressed to G.M., G.R. or M.G.

Peer review information Primary Handling Editor: Christoph Schmitt.

Reprints and permissions information is available at www.nature.com/reprints.

Publisher's note Springer Nature remains neutral with regard to jurisdictional claims in published maps and institutional affiliations.

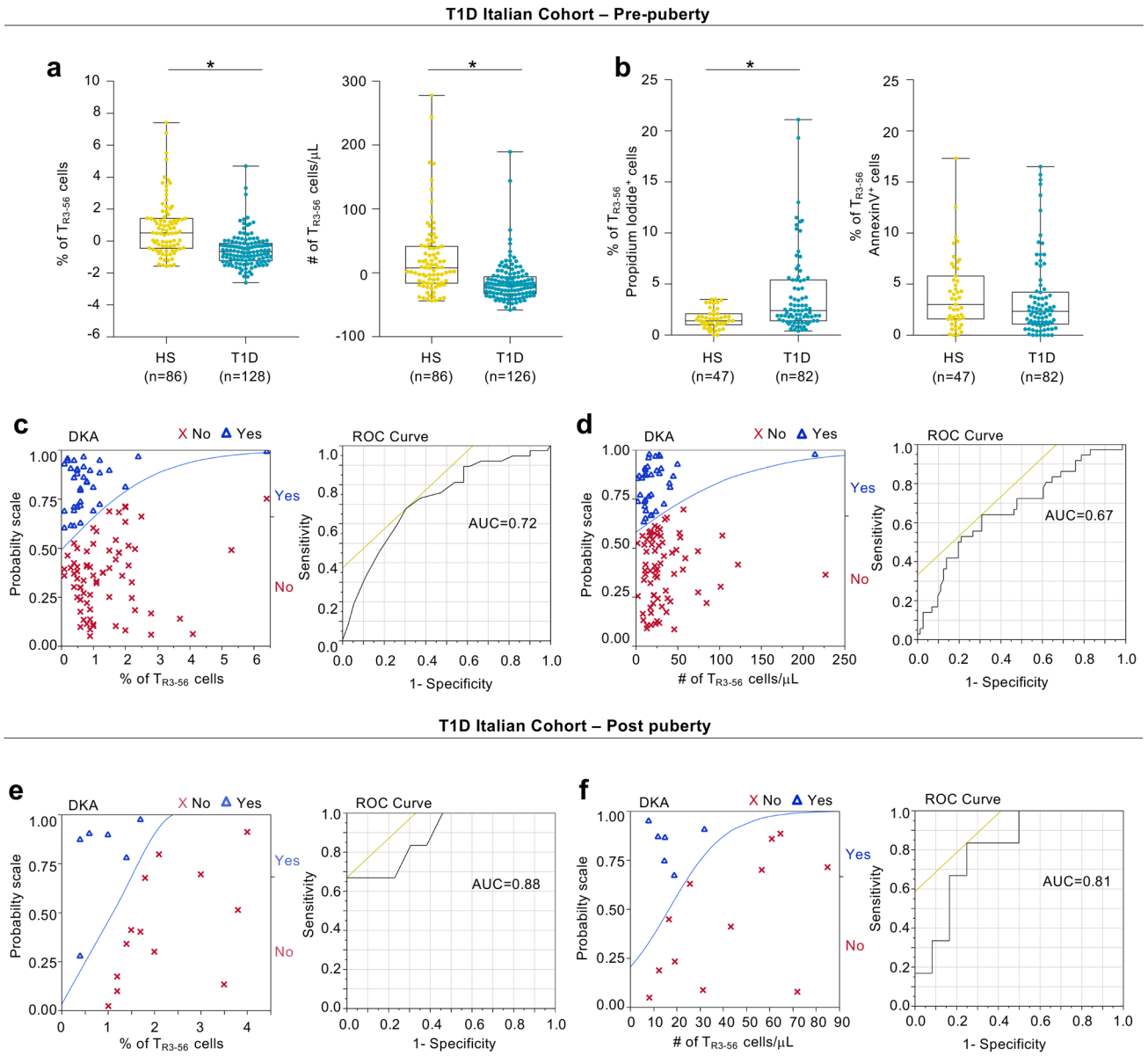

Extended Data Fig. 1 | T_{R3-56} cell enumeration predicts residual β-cell function and DKA in pre-puberty T1D subjects at disease onset. a, Box plots indicate the percentage (left) and absolute number (right) of circulating T_{R3-56} cells in pre-puberty T1D subjects at disease onset from Italian cohort compared with healthy subjects, after adjustment for age, sex and BMI. Data are presented as box plots (min, max, median, and 25th and 75th percentiles), each dot represents a individual subjects (n=86 healthy subjects; n=128 T1D for percentage of T_{R3-56} cells and n=126 T1D for absolute number of T_{R3-56} cells). *p<0.0001 by two-tailed Mann-Whitney U-test. **b**, Box plots indicate the percentage of necrotic (left) and apoptotic (right) rate of circulating T_{R3-56} cells in healthy subjects (n=47) and T1D children at disease onset (n=82) from Italian cohort. Data are presented as box plots (min, max, median, and 25th and 75th percentiles), each dot represents a individual subjects. *p<0.0001 by two-tailed Mann-Whitney U-test. **c**, Left, logistic regression modeling shows that percentage of T_{R3-56} cells predicts the presence or absence of DKA in pre-puberty T1D subjects at diagnosis (n=128) from Italian cohort. T1D subjects were dichotomized on the basis of the presence (Yes) or absence (No) of DKA at disease diagnosis. Low numbers of T_{R3-56} cells at diagnosis associated with presence of DKA. Right, ROC curve of the model-based prognostic scores of T_{R3-56} cells for the presence of DKA. AUC=0.72. **d**, Left, logistic regression modeling shows that absolute number of T_{R3-56} cell counts predicts the presence or absence of DKA in pre-puberty T1D subjects at diagnosis (n=126) from Italian cohort. Right, ROC curve of the model-based prognostic scores of T_{R3-56} cells for the presence of DKA. AUC=0.67. **e**, Left, logistic regression modeling shows that percentage of circulating T_{R3-56} cells predicts the presence or absence of DKA in post-puberty young adults T1D (n=19) from Italian cohort. Right, ROC curve of the model-based prognostic scores of T_{R3-56} cells for the presence of DKA. AUC=0.88. **f**, Left, logistic regression modeling shows that absolute number of T_{R3-56} cells predicts presence of DKA in post-puberty young adults T1D (n=18) from Italian cohort. Right, ROC curve of the model-based prognostic scores of T_{R3-56} cells for the presence of DKA. AUC=0.81.

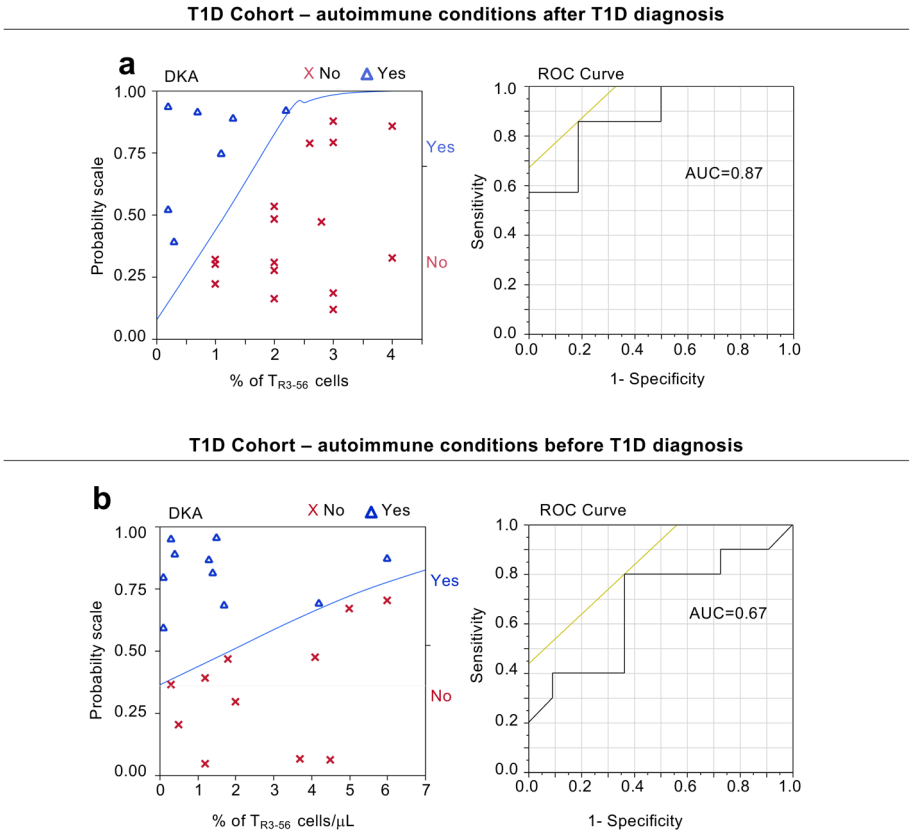

Extended Data Fig. 2 | T_{R3-56} cells in T1D subjects with other autoimmune diseases. a, Left, logistic regression modeling shows that percentage of T_{R3-56} cells predicts the presence or absence of DKA in children (n=23) that developed after diagnosis of T1D another autoimmune conditions (CD or AIT). T1D subjects were dichotomized on the basis of the presence (Yes) or absence (No) of DKA at disease diagnosis. Right, ROC curve of the model-based prognostic scores of T_{R3-56} cells for the presence of DKA. AUC=0.87. **b**, Left, logistic regression modeling shows that peripheral frequency of T_{R3-56} cells associated with presence of DKA in children (n=21) that at T1D diagnosis are already affected by other autoimmune conditions. Right, ROC curve of the model-based prognostic scores of T_{R3-56} cells for the presence of DKA. AUC=0.67.

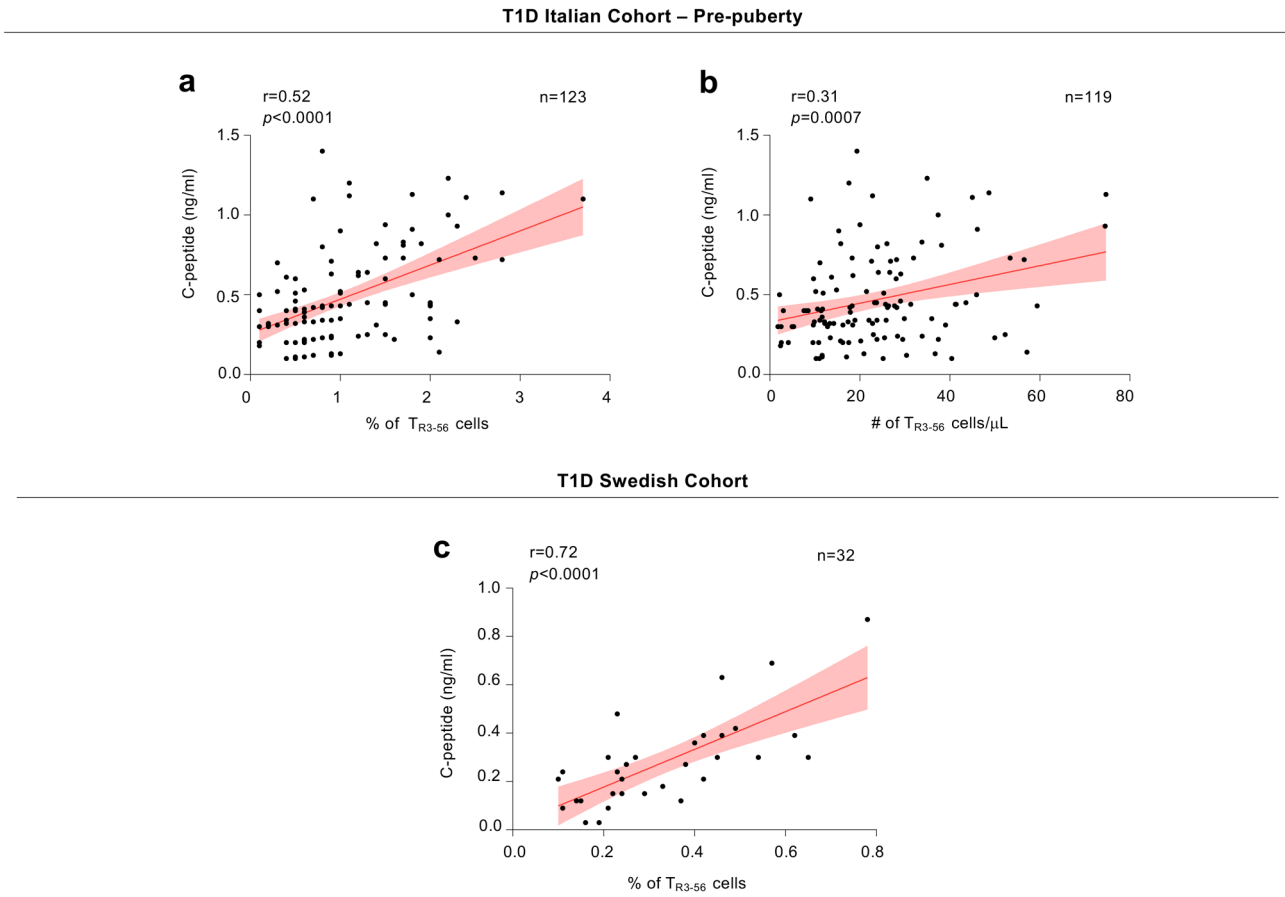

Extended Data Fig. 3 | Correlation between $T_{R3\text{-}56}$ cells and fasting C-peptide in the absence of outliers. a, Scatter plot showing statistical correlation between frequency of $T_{R3\text{-}56}$ cells and fasting C-peptide in the absence of $T_{R3\text{-}56}$ cell outliers (n=5) in pre-puberty T1D subjects (n=123) at disease onset from Italian cohort. Red line indicates regression line and shading indicates confidence interval. r=0.52, $p<0.0001$ by two-tailed Pearson's correlation. **b**, Scatter plot showing statistical correlation between absolute numbers of $T_{R3\text{-}56}$ cells and C-peptide in the absence of $T_{R3\text{-}56}$ cell outliers (n=7) in pre-puberty T1D subjects (n=119) at disease onset from Italian cohort. Red line indicates regression line and shading indicates confidence interval. r=0.31, $p=0.0007$ by two-tailed Pearson's correlation. **c**, Scatter plot showing positive correlation between the frequency of circulating $T_{R3\text{-}56}$ cells and serum levels of fasting C-peptide in absence of $T_{R3\text{-}56}$ outliers (n=4) in Swedish cohort of T1D children (n=32) at disease onset; Red line indicates regression line and shading indicates confidence interval. r=0.72, $p<0.0001$ by two-tailed Pearson's correlation. To identify outliers ROUT (Q=0.1%) method has been applied.

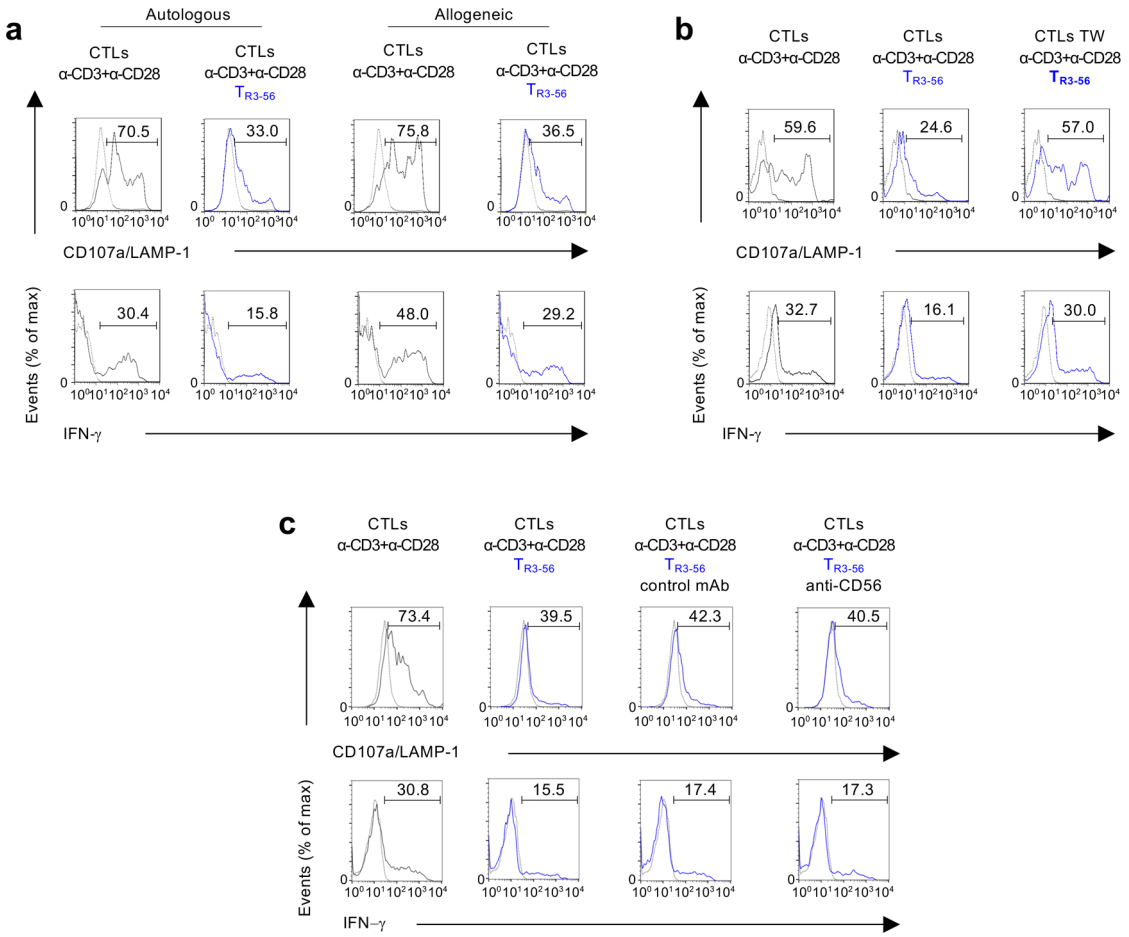

Extended Data Fig. 4 | T_{R3-56} cells suppress CD107a/LAMP-1 and IFN-γ in both autologous and allogeneic conditions, require cell-to-cell contact and is independent from CD56 molecules. a, Representative flow cytometry histograms showing CD107a/LAMP-1 and IFN-γ staining of CTLs after 4 hours of culture with anti-CD3 plus anti-CD28 microbeads alone (grey), in the presence of autologous or allogeneic T_{R3-56} cells (blue) as indicated. Dotted lines indicate unstimulated CTLs. Numbers indicate percentage of positive cells. Data are from one representative experiment out of four. **b**, Representative flow cytometry histograms showing CD107a/LAMP-1 and IFN-γ staining of CTLs cultured for 4 hours with anti-CD3 plus anti-CD28 microbeads alone (grey), in the presence of T_{R3-56} cells or when T_{R3-56} cells were separated by transwell (TW) plate system (as indicated). Dotted lines indicate unstimulated CTLs. Numbers indicate percentage of positive cells. Data are from one representative experiment out of six. **c**, Representative flow cytometry histograms showing CD107a/LAMP-1 and IFN-γ staining of CTLs after 4 hours of culture with anti-CD3 plus anti-CD28 microbeads alone (grey), or in the presence of T_{R3-56} cells (blue), either in the presence of the control 345.134 IgG2a or the anti-CD56 neutralizing mAb, as indicated. Dotted lines indicate unstimulated CTLs. Numbers indicate percentage of positive cells. Data are from one representative experiment out of three.

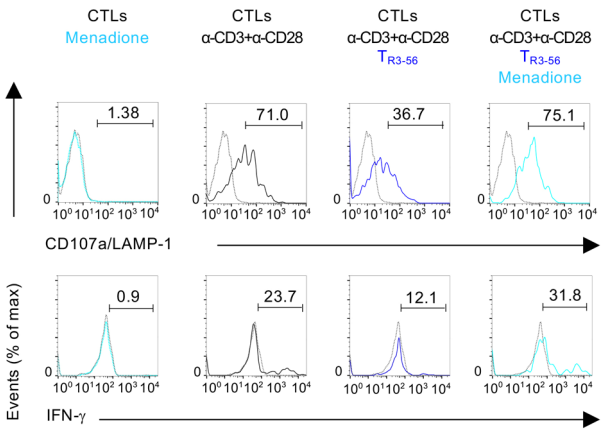

Extended Data Fig. 5 | Menadione pre-treated CTLs are resistant to $T_{R3\text{-}56}$ cell suppressive activity. CD107a/LAMP-1 and IFN-γ staining of CTLs cultured for 4 hours in the presence or absence of anti-CD3 plus anti-CD28 microbeads alone or in the presence of $T_{R3\text{-}56}$ cells; light blue lines indicate CTLs pre-treated for 15 minutes with 0.05 mM menadione. Dotted lines indicate unstimulated cells. Numbers indicate percentage of positive cells. Data are from one representative experiment out of six.

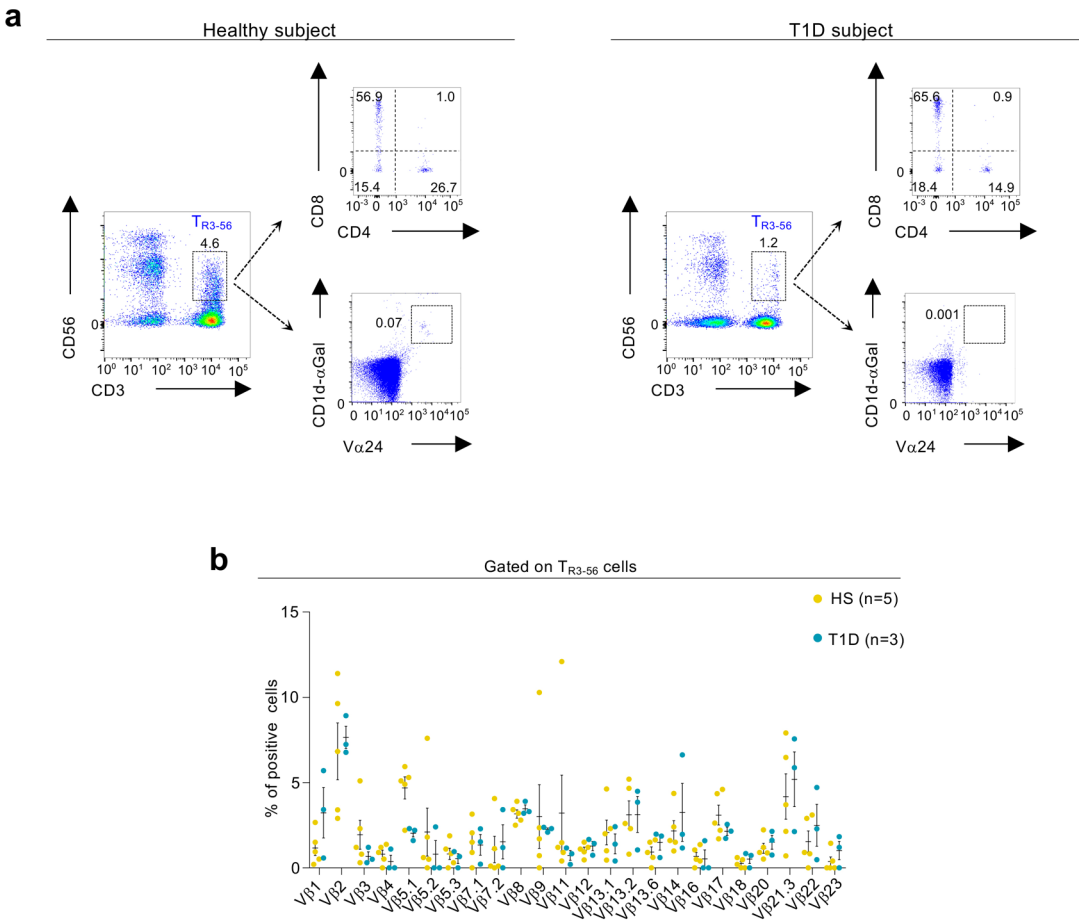

Extended Data Fig. 6 | Phenotype of peripheral TR3-56 cells in healthy and T1D subjects. a, Representative flow-cytometry plots showing the gating strategy used to evaluate the expression of CD4 and CD8 on $T_{R3\text{-}56}$ cells (upper panels) and the frequency of invariant (i)NKT cells, evaluated by Vα24 expression and CD1d tetramers loaded with a-Galactosyl ceramide (CD1d-aGal) binding on $T_{R3\text{-}56}$ lymphocytes (lower panels) on both healthy and T1D at-onset subjects, as indicated. Numbers in plots indicate percent of positive cells. **b**, Column bar showing the TCR Vβ family expression in TR3-56 cells from healthy subjects (yellow) and T1D children (turquoise) at diagnosis, as indicated. Data are from n=5 healthy subjects and n=3 T1D subjects. Data are expressed as mean ± SEM. No statistical significance differences are identified by two-way ANOVA-corrected for multiple comparison using Bonferroni test ($p > 0.9999$).

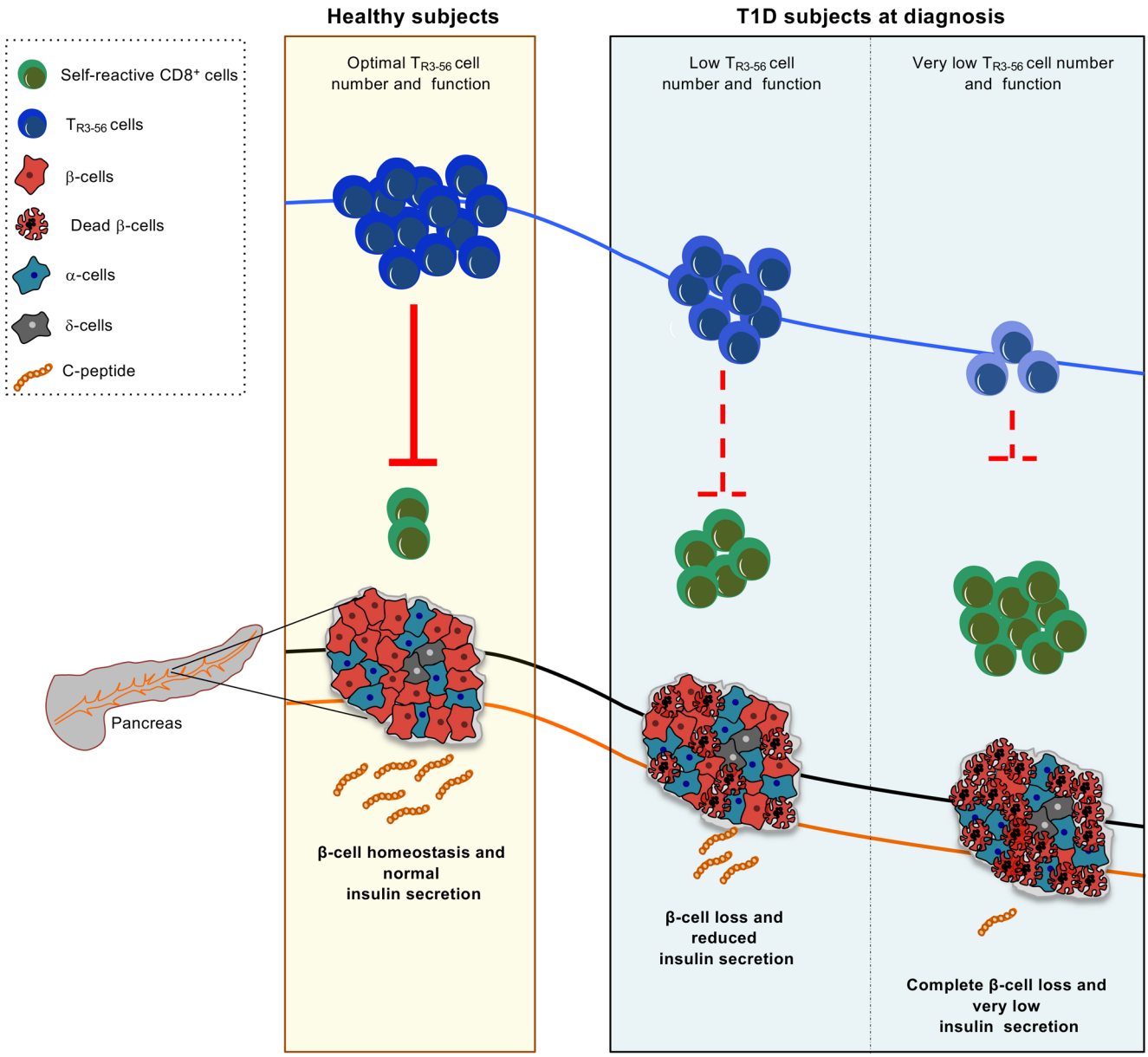

Extended Data Fig. 7 | Hypothetic model showing the regulatory function of TR3-56 cells and β-cell integrity in healthy and autoimmune conditions. In healthy subjects, normal number and suppressive function of T_{R3-56} cells control self-reactive $CD8^+$ T cells (green), possible contributing to maintenance of immune self-tolerance and insulin production by live β-islet cells (red). Right, in autoimmune T1D, a lower frequency and a reduced functional capacity of T_{R3-56} cells correlated with reduced β-cell mass, reduced serum levels of C-peptide and progressive lost of immunological self-tolerance. The schematic model was prepared using the Motifolio Scientific Illustration Toolkit (Motifolio).

nature research

Corresponding author(s): Mario Galgani, Giuseppina Ruggiero and Giuseppe Matarese

Last updated by author(s): Dec 30, 2019

Reporting Summary

Nature Research wishes to improve the reproducibility of the work that we publish. This form provides structure for consistency and transparency in reporting. For further information on Nature Research policies, see Authors & Referees and the Editorial Policy Checklist.

Statistics

For all statistical analyses, confirm that the following items are present in the figure legend, table legend, main text, or Methods section.

n/a	Confirmed
☐	☒ The exact sample size (*n*) for each experimental group/condition, given as a discrete number and unit of measurement
☐	☒ A statement on whether measurements were taken from distinct samples or whether the same sample was measured repeatedly
☐	☒ The statistical test(s) used AND whether they are one- or two-sided *Only common tests should be described solely by name; describe more complex techniques in the Methods section.*
☒	☐ A description of all covariates tested
☐	☒ A description of any assumptions or corrections, such as tests of normality and adjustment for multiple comparisons
☐	☒ A full description of the statistical parameters including central tendency (e.g. means) or other basic estimates (e.g. regression coefficient) AND variation (e.g. standard deviation) or associated estimates of uncertainty (e.g. confidence intervals)
☒	☐ For null hypothesis testing, the test statistic (e.g. *F*, *t*, *r*) with confidence intervals, effect sizes, degrees of freedom and *P* value noted *Give P values as exact values whenever suitable.*
☒	☐ For Bayesian analysis, information on the choice of priors and Markov chain Monte Carlo settings
☐	☒ For hierarchical and complex designs, identification of the appropriate level for tests and full reporting of outcomes
☐	☒ Estimates of effect sizes (e.g. Cohen's *d*, Pearson's *r*), indicating how they were calculated

Our web collection on statistics for biologists contains articles on many of the points above.

Software and code

Policy information about availability of computer code

Data collection	Data was collected in Microsoft Excel. Transcriptome of isolated human cell populations was quantified through microarray-based human Affymetrix Clariom S Assays (Eurofins Genomics), which provides extensive coverage of all known well-annotated genes (21448 gene probes for 19525 annotated unique genes). For NGS analysis of cell populations isolated from children, RNA sequencing was performed on single-end 75 bp mode on NextSeq 500 (Illumina, San Diego, CA) and number of reads ranged from 29.1x106 to 32.5x106.
Data analysis	Biospecimen analyses: GraphPad Prism7 and JMP software. For microarray, the raw intensity values were background corrected, log2 transformed and quantile normalized using the Robust Multi-array average (RMA) algorithm. Data were imported and analysed using MultiExperimentViewer (MeV). Sample similarity was described by multivariate Principal Component Analysis (PCA) and Pearson correlation. For supervised sample clustering, significant genes were selected by one-way ANOVA, followed by Pearson correlation. In order to identify a TR3-56 cell specific gene expression pattern, we selected genes for having a consistent log2 fold change (either > +1 or < -1) compared to all other evaluated populations (NK, CD3+CD56- and CD8+ cells) and a significant Student's t-test ($p<0.05$) for all three comparisons: TR3-56 vs NK, TR3-56 vs CD3+CD56- and TR3-56 vs CD8+ T cells. For NGS, raw data were processed by Bcl2Fastq 2.0.2 version of the Illumina pipeline for both format conversion and de-multiplexing and lower quality bases and adapters were removed by ERNE and Cutadapt software. Reads were aligned on reference GRCh38 genome/ transcriptome with STAR and DESeq2 was used to perform comparisons between expression levels of genes and transcripts. Normalization was performed using the median-of-ratios method and statistical significance determined using a Wald test.

For manuscripts utilizing custom algorithms or software that are central to the research but not yet described in published literature, software must be made available to editors/reviewers. We strongly encourage code deposition in a community repository (e.g. GitHub). See the Nature Research guidelines for submitting code & software for further information.

Data

Policy information about availability of data

All manuscripts must include a data availability statement. This statement should provide the following information, where applicable:

- Accession codes, unique identifiers, or web links for publicly available datasets
- A list of figures that have associated raw data
- A description of any restrictions on data availability

The data that support the findings of this study are available from the corresponding author upon request. Transcriptional data of TR3-56, NK, CD3+CD56-, CD8+ cells are in the GEO database with accession code GSE106082. Transcriptional data of TR3-56 from T1D and healthy children are in the GEO database with accession code GSE134916.

Field-specific reporting

Please select the one below that is the best fit for your research. If you are not sure, read the appropriate sections before making your selection.

☒ Life sciences ☐ Behavioural & social sciences ☐ Ecological, evolutionary & environmental sciences

For a reference copy of the document with all sections, see nature.com/documents/nr-reporting-summary-flat.pdf

Life sciences study design

All studies must disclose on these points even when the disclosure is negative.

Sample size	For in vitro experiments sample size was determined empirically, at least two independent experiments were performed.
Data exclusions	No data were excluded.
Replication	The experimental findings were reliably reproduced.
Randomization	Human samples were allocated in two groups to separate healthy subjects from T1D individuals; also, human samples from different independent T1D cohorts were dicothomitized on the basis of C-peptide levels and presence of diabetic ketoacidosis (DKA).
Blinding	For the studies on TR3-56 cell frequency and function the analysis were performed blinded.

Reporting for specific materials, systems and methods

We require information from authors about some types of materials, experimental systems and methods used in many studies. Here, indicate whether each material, system or method listed is relevant to your study. If you are not sure if a list item applies to your research, read the appropriate section before selecting a response.

Materials & experimental systems

n/a	Involved in the study
☐	☒ Antibodies
☒	☐ Eukaryotic cell lines
☒	☐ Palaeontology
☒	☐ Animals and other organisms
☐	☒ Human research participants
☒	☐ Clinical data

Methods

n/a	Involved in the study
☒	☐ ChIP-seq
☐	☒ Flow cytometry
☒	☐ MRI-based neuroimaging

Antibodies

Antibodies used	All antibodies used were reported in the material method section of the manuscript.
Validation	High-quality monoclonal antibodies were chosen based on the validation statements for human and application (flow cytometry, co-culture experiments) on the manufacturer's website.

Human research participants

Policy information about studies involving human research participants

Population characteristics	All population characteristics were reported in the material method section of the manuscript and in the Supplementary Tables.
Recruitment	Subjects were recruited at the Dipartimento di Scienze Mediche Traslazionali, Sezione di Pediatria University of Naples ''Federico II' ; at European Laboratory for the Investigation of Food-Induced Disease, University of Naples, "Federico II" and at Crown Princess Victoria Children´s Hospital, University Hospital, Linköping, Sweden.
Ethics oversight	The study was approved by Istitutional Review Board of the Ethics Committee of University of Naples "Federico II" (Prot. N. 200/16 and N.161/18) and by the Research Ethics Committee of Linköping University (Dnr 02-482).

Note that full information on the approval of the study protocol must also be provided in the manuscript.

Flow Cytometry

Plots

Confirm that:

☐ The axis labels state the marker and fluorochrome used (e.g. CD4-FITC).

☒ The axis scales are clearly visible. Include numbers along axes only for bottom left plot of group (a 'group' is an analysis of identical markers).

☐ All plots are contour plots with outliers or pseudocolor plots.

☒ A numerical value for number of cells or percentage (with statistics) is provided.

Methodology

Sample preparation	CTLs, TR3-56, CD8+, NK, CD3+CD56- and CD4+ were obtained from PBMCs and isolated either from healthy donors orT1D subjects.
Instrument	Data acquisition was performed using BD Biosciences FACSCanto II . Cells were flow-sorted by using FACS Jazz (BD Biosciences).
Software	Flow cytometric analysis were acuired by DIVA software (BD Bioscience) and performed with the FlowJo analysis software V10 (FlowJo, LLC).
Cell population abundance	Purity of sorted cell population was at least 95%, determined by flow-cytometry analysis post-sorting.
Gating strategy	For flow cytometry experiments the gating strategy was shown in the Supplementary Fig. 4.

☒ Tick this box to confirm that a figure exemplifying the gating strategy is provided in the Supplementary Information.